

P
2mif

X-910-74-20

PREPRINT

NASA TM X-70633

A MULTI-SENSOR ANALYSIS OF NIMBUS 5 DATA ON 22 JANUARY 1973

L. J. ALLISON
E. B. RODGERS
T. T. WILHEIT
R. WEXLER

(NASA-TM-X-70633) A MULTI-SENSOR ANALYSIS
OF NIMBUS 5 DATA ON 22 JANUARY 1973

N74-22115

(NASA) 58 p HC \$6.00

CSCL 14B

59

Unclass

G3214 38363

JANUARY 1974

GSFC

GODDARD SPACE FLIGHT CENTER

GREENBELT, MARYLAND

I

For information concerning availability
of this document contact:

Technical Information Division, Code 250
Goddard Space Flight Center
Greenbelt, Maryland 20771

(Telephone 301-982-4488)

A MULTI-SENSOR ANALYSIS OF NIMBUS 5 DATA

ON 22 JANUARY 1973

L. J. Allison
E. B. Rodgers*
T. T. Wilheit
R. Wexler

January 1974

GODDARD SPACE FLIGHT CENTER
Greenbelt, Maryland

*Environmental Research and Technology, Inc., Lexington, Massachusetts 02173.

A MULTI-SENSOR ANALYSIS OF NIMBUS 5 DATA
ON 22 JANUARY 1973

L. J. Allison
E. B. Rodgers
T. T. Wilheit
R. Wexler

ABSTRACT

The Nimbus 5 meteorological satellite carried aloft a full complement of radiation sensors, the data from which were analyzed and intercompared during orbits 569-570 on 22 January 1973. The Electrically Scanning Microwave Radiometer (ESMR) which sensed passive microwave radiation in the 19.35 GHz region, delineated rain areas over the ocean off the U.S. east coast, in good agreement with WSR-57 and FPS-77 radar imagery and permitted the estimation of rainfall rates in this region. Residual ground water in the lower Mississippi Valley, which resulted from abnormal rainfall in previous months, was indicated under clear sky conditions by soil brightness temperature values in the Nimbus 5 ESMR and U.S. Air Force Data Acquisition and Processing Program (DAPP) IR data. The Temperature-Humidity Infrared Radiometer (THIR, $6.7\mu\text{m}$ and $11\mu\text{m}$) showed the height and spatial configuration of frontal clouds along the east coast and outlined the confluence of a polar jet stream with a broad sub-tropical jet stream along the U.S. Gulf Coast. Temperature profiles from three vertical temperature sounders, the Infrared Temperature Profile Radiometer (ITPR), the Nimbus E Microwave Spectrometer (NEMS) and the Selective Chopper Radiometer (SCR) were found to be in good agreement with related radiosonde ascents along orbit 569 from the sub-tropics to the Arctic Circle.

PRECEDING PAGE BLANK NOT FILMED

CONTENTS

	<u>Page</u>
ABSTRACT	iii
INTRODUCTION	1
THE NIMBUS 5 ELECTRICALLY SCANNING MICROWAVE RADIOMETER (ESMR) EXPERIMENT	1
FUNDAMENTAL PHYSICAL RELATIONSHIPS	2
THE ESMR INSTRUMENT AND SELECTED DATA EXAMPLES	3
METEOROLOGICAL ANALYSIS OF 22 JANUARY 1973	4
HYDROLOGICAL AND OTHER APPLICATIONS	9
THE NIMBUS 5 TEMPERATURE-HUMIDITY INFRARED RADIOMETER (THIR) EXPERIMENT AND DATA ANALYSIS	10
THE NIMBUS 5 VERTICAL TEMPERATURE SOUNDERS AND DATA ANALYSIS	11
CONCLUSION	12
ACKNOWLEDGMENTS	15
REFERENCES	16

PRECEDING PAGE BLANK NOT FILMED

A MULTI-SENSOR ANALYSIS OF NIMBUS 5 DATA ON 22 JANUARY 1973

INTRODUCTION

Nimbus 5, launched on 11 December 1972, is a research and development satellite which carried aloft the Electrically Scanning Microwave Radiometer (ESMR), a promising new tool for global synoptic weather analysis. This instrument recorded microwave radiometric measurements through clouds and inferred new meteorological and hydrological parameters that were not detectable by previous visible or infrared satellite sensors (Skidmore and Purdom, 1973).

The purpose of this paper is to describe the ESMR experiment and make multi-sensor data comparisons with the Temperature-Humidity Infrared Radiometer (THIR), the Infrared Temperature Profile Radiometer (ITPR), the Nimbus E Microwave Spectrometer (NEMS), the Selective Chopper Radiometer (SCR), meteorological radar and radiosonde data close to satellite-overpass time over the eastern United States and interpret their meteorological usefulness during orbits 569-570 on 22 January 1973.

THE NIMBUS 5 ELECTRICALLY SCANNING MICROWAVE RADIOMETER (ESMR) EXPERIMENT

The ESMR was designed to measure earth and atmospheric radiation in the 19.35 GHz (1.55 cm) region from a polar orbit at approximately 1100 km altitude. The purposes in flying this experiment were to record and map passive microwave radiation patterns (in brightness temperature, T_B), for the delineation of areas of precipitation, to derive cloud liquid water content over the oceans, and, by comparison with simultaneous observations in the visible and infrared channels, to differentiate between cirrus and other ice crystal clouds and thick water droplet clouds.

Other aims of this research program were to observe and demarcate areas of sea ice and open sea in the polar regions regardless of cloud cover and to test the feasibility of inferring soil moisture providing that no heavy clouds exist over the area of interest.

NASA Convair 990 flights with the "aircraft prototype" model of ESMR by Catoe et al., 1967; Nordberg et al., 1969; Gloersen et al., 1972, 1973 (a), (b), and (c); Schmugge et al., 1972; and Wilheit et al., 1972 had established the feasibility of the basic microwave measurements over the oceans, land and sea ice, prior to the Nimbus 5 launch, and also provided check-of-calibration "ground truth" observations under the satellite after launch.

The application of passive microwave techniques to the ocean surface has been documented by Paris, 1969, 1971; Hollinger, 1971; Ross et al., 1970; and Nordberg et al., 1971. These studies related the microwave signature of the ocean and atmosphere to sea state, surface temperature, salinity, and atmospheric moisture (U.S. Department of Commerce, 1971).

Martin and Scherer, 1973, in their review of present satellite rainfall estimate methods, document the value of making rainfall estimates globally. They note that precipitation is a sensitive indicator of the amount and distribution of the release of latent heat of condensation, the upward mass flux and the spatial organization of convection. The accurate estimate of precipitation is important in studies of the heat and water budget over convective clouds with special emphasis during the Data Systems Test and GATE in 1974 (GARP Project, 1973). Since previous satellite sensor systems cannot directly detect rain in its liquid or near-frozen state (Follansbee, 1973), the ESMR data was needed to fill the gap in this vital global observational area.

FUNDAMENTAL PHYSICAL RELATIONSHIPS

In the microwave region, Planck's formula for the spectral intensity of thermal radiation emitted by a surface is given by the Rayleigh-Jeans Approximation:

$$I(\lambda, T) = \frac{e^2 \pi c k T}{\lambda^4} \quad (\text{Leighton, 1959})$$

where:

T = Thermodynamic temperature

k = Boltzmann's constant

λ = wavelength

c = velocity of light

e = emissivity of surface

I = emission per unit area per unit wavelength interval

T_B = brightness temperature

I is directly proportional to the temperature, T, hence the thermal radiation is approximately proportional to the product of the emissivity and the actual temperature,

$$eT = \frac{I_{\lambda} \lambda^4}{2 \pi c k}$$

Where:

$$T_B = e T$$

The ESMR can measure brightness temperatures over the 180 K range, extending from 120 K to 300 K. Since the ocean has a low surface emissivity of 0.4 at 19.35 GHz, as compared with 0.85 to 0.95 and greater for non-vegetating ground surface, the T_B values under clear sky conditions are expected to range from 120 K to 160 K, depending on latitudinal variation of water content. Microwave radiation can penetrate non-raining clouds, although there is some minor attenuation. Large cloud droplets and rain (below the freezing level, generally <4.5 km) in the atmosphere have an enhanced absorption effect due to an effective size dimension comparable to wavelength divided by the large index of refraction of water at microwave frequencies and are delineated by T_B values of 160 to 260 K over an ocean background (Gunn and East, 1954; Wilheit, 1972; Aerojet ElectroSystems Co., 1973).

Since the imaginary part of the dielectric constant of ice is so small at microwave frequencies, the absorption coefficient of ice crystals within cirrus cloud formations is negligible. At the ESMR frequency, there is no sensitivity to ocean salinity, but there is some effect at the nadir due to ocean roughness, streaks, and white cap cover (Nordberg, et al., 1971; Porter and Wentz, 1972).

THE ESMR INSTRUMENT AND SELECTED DATA EXAMPLES

The ESMR consists of a microwave receiver which operates in the Dicke mode to eliminate low frequency noise, associated electronics, and an electrically-scanned planar array antenna capable of receiving one polarization. The 90 by 90 cm radiometer antenna, which was deployed after launch, scans the earth every four seconds and views 50° either side of nadir in 78 steps with some overlap (Figure 1). The radiometric scanning process is controlled by an on-board computer which permits the recording of brightness temperature within a NEAT of approximately 2 K from a 25 km scan spot at nadir to a 45 x 165 km scan spot at 50° nadir angle (Wilheit, 1972). A cold reference temperature is obtained by using a sky horn which looks out at the cold radiant temperature of space. This space temperature was noted to be approximately 3 K in the 19.35 GHz frequency range. By monitoring two reference loads in the radiometer, and the

cold horn reference temperature, the observed radiometric temperature can be corrected to obtain system absolute brightness temperatures within ± 1 K. The microwave radiation detected at the spacecraft is formatted on board by the Versatile Information Processor (VIP) and stored with the atmospheric and other sensor data on the VIP track of the High Data Rate Storage System (HDRSS) tape recorder. Data are telemetered to the ground at Fairbanks, Alaska and Rosman, North Carolina, and transmitted to GSFC for research studies.

The following pictures contain several examples of Nimbus 5 ESMR data obtained from "quick-look" photofacsimile processing. Figure 2 shows three global montages of individual orbits 735 through 747 recorded on 4 February 1973. Three dynamic ranges are shown: montage 1 (138 to 210 K), montage 2 (194 to 256 K), and montage 3 (254 to 290 K). Montage 1 shows rainfall areas and variations in atmospheric moisture but no information is discernable over the dark land areas. Montage 2 indicates areas of intense rainfall over the oceans and shows contrasts between first year ice formations (dark) and older ice and snow (light). For further details on more recent Nimbus 5 ESMR sea ice detection results, see Gloersen, et al., 1973, a, b, and c; Wilheit, et al., 1972; and Campbell, et al., 1973.

Montage 3 shows areas of heavy rainfall over oceans, high soil moisture, and snow cover over land areas. Figure 3 shows three examples of mid-latitudinal frontal rain over the Pacific and Atlantic Ocean during December 1972. Note the narrow dark line of rain within the pre-frontal squall line in (b) and the more diffuse rain areas shown in the warm front (a) and occluded front (c). A more comprehensive discussion of other synoptic cases using ESMR imagery may be found in studies by Wilheit, et al., 1973; Theon, 1973; and Sabatini and Merritt, 1973.

In order to verify the exact location of rain clouds in a frontal system over water off the U.S. east coast, a determined effort was made to collect nearly simultaneous ground weather radar data, to coincide with the Nimbus 5 over-flight during orbit 569 on 22 January 1973. A discussion of the meteorological results of this correlative analysis is found in the next section.

METEOROLOGICAL ANALYSIS OF 22 JANUARY 1973

The 1800 GMT NMC surface weather chart (Figure 4) shows the location of an active cold front, oriented NE/SW off the east coast of the U.S. which was moving southeastward through central Florida. Cloud remnants of the associated decaying occlusion which was located over the mid-west and Great Lakes region were also recorded between 1600-1800 GMT by the U.S. Air Force DAPP, ATS-3 and Nimbus 5 (THIR) satellites (Figures 5a, 5b, and 5c).

A Nimbus 5 ESMR photofacsimile picture of orbit 569 and the associated 1:5 Million Mercator digital grid print map are shown in Figure 6(a) and (b) respectively. Note that the Great Lakes appear quite cold (150 to 180 K, white tone) even through overcast clouds, and the heavy frontal rain off the southeast U.S. coast appears dark grey (160 to >240 K). The National Weather Service radar summary for 1640 GMT, 22 January 1973 (Figure 7) indicates 25 to 41,000 ft. tops over a line of thunderstorms through central Florida while lower heights (20-22,000 ft.) were recorded over lighter rainshowers further to the north. Scattered rain and snow showers are shown to the west over the north-central Mississippi Valley and Great Lakes region. These showers are within the slowly-filling occlusion which appears as light grey in Figure 6a(1).

A comprehensive effort was made to obtain all available WSR-57 weather radar polaroid pictures taken within 10 minutes of Nimbus 5 satellite passage over the east coast. An example of data recorded at Daytona Beach, Florida is shown in Figure 8(a). The radar images were carefully relocated on a 1:2.5 Million Mercator map base (Figure 8b). Note the overlap of radar echoes (darker zip-tones) between Wilmington-Hatteras, North Carolina and Daytona Beach-Tampa-Key West, Florida. A large radar gap appears between 30° to 32°N just east of the Waycross, Georgia radar site. However, the location of warm ESMR brightness temperatures $T_B = 180$ to >220 K in the frontal zone shows the rain to be continuous in that region (Figure 8c). There is a good relationship between the ESMR brightness data (> 170 K) and radar rainfall echoes over the water southwest of Wilmington, North Carolina and Tampa, Florida. Lake Okeechobee ($T_B = 230$ to 240 K), located at approximately 27°N, 80°W in south-central Florida and the Florida coastline ($T_B = 200$ to 220 K) were used to more accurately position the ESMR data, which was in error by 1° lat-long. Figure 8d shows a 1:2.5 Million Mercator digital grid print map of Nimbus 5 THIR(11 μ m) data over the same area. A high cloud cluster, as indicated by T_B values < 230 K in the 11 μ m imagery over the area of the radar gap off the Georgia coast implies the presence of rainshowers in that area. The high cloudiness at point A is a result of cirrus blowoff from thunderstorms in the vicinity of the sub-tropical jet stream. Note that these ice crystal clouds are not indicated by the ESMR data in Figure 8c. The other areas of cold T_B values in Figure 8d (< 230 K, indicated by dots) generally overlay rain echoes in Figure 8b, and warmer ESMR T_B values in Figure 8c (> 170 K). There is a generalized inverse relationship between the ESMR brightness temperatures of frontal rain clouds over water and the 11 μ m data. This pertains similarly to the post-frontal clearer-sky subsidence area off the South Carolina coast (30° to 33°N) and eastern Gulf of Mexico.

As a result of close coordination with Detachment 11, 6th Weather Wing, Air Weather Service at Cape Kennedy, Florida, FPS-77 radar data were recorded at 1641 GMT within two minutes of Nimbus 5 overflight in that area (Figure 9a).

Four levels of rainfall rate, in shades of grey, were obtained by using PPI polaroid pictures with the following criteria: 45 dB = 2 inches per hour, 40 dB = 1 inch (25.4 mm) per hour, 35 dB = 0.5 inch (12.7 mm) per hour, 30 dB = 0.3 inch (7.6 mm) per hour. Note the small area of 0.3 inch per hour radar echoes in the one degree square in the top right hand corner of Figure 9a and the large area of ESMR T_B values 200 to 220 K in Figure 9b. At a range of 75-100 miles, with a 0.5 degree elevation angle, the FPS-77 can only detect precipitation at the 10-12,000 level due to the earth's curvature. This height was the approximate freezing level for the radar gap area. It is evident that the ESMR data provides more qualitative rainfall information than the ground weather radar which has its physical limitations due to slant range, elevation angle, cloud dropsize distribution, and other attenuation factors (Battan, 1959). The 0.5 to 1 inch per hour isolines over water, east of Cape Kennedy in Figure 9a, overlay the 170 to 200 K brightness values in Figure 9b. The 1 to 2 inch per hour rainfall isolines extending over land southwestward from Cape Kennedy in Figure 9a are not clearly indicated in the ESMR brightness temperatures patterns in Figure 9b. This may be due to the failure of the thin line of frontal thunderstorms to fill the whole field of view and/or mis-location of the ESMR scan spots by the computer program. The effect of the complicated patterns of background radiance of the small lakes, swampland, forests, cultivated soils and vegetation in Central Florida must be measured daily under clear sky conditions by ESMR in order to understand the changes in ESMR brightness values during rainy periods. This makes the determination of actual rainfall rates over land extremely difficult.

A more detailed empirical study of nearly simultaneous ESMR and weather radar data over water was made using rainfall rates obtained from the Video Integrator Processor (VIP) system on the WSR-57 radar set at Miami, Florida. In this analysis, data sampling of the ESMR brightness values were obtained from the Nimbus 5 brightness temperature tape which gives time, latitude and longitude and T_B values for all 50 scan positions from a limit of 30° left to 30° right of nadir perpendicular to the spacecraft forward velocity vector. The instantaneous field of view at the scan position near nadir is 25 x 25 km degrading to approximately 30 x 40 km at 30° off nadir.

The VIP processes the radar's logarithmic receiver output to show six levels of rainfall intensity up to a 125 mile nautical mile range. The six intensity levels are contoured on the radar PPI scope for all echoes by use of a grey shade scale. Rainfall rates less than 2.5 mm per hour between 2.5 to 12.7 mm per hour and between 12.7 to 25.4 mm per hour are shaded grey, white and black respectively. For rainfall rates between 25.4 to 50.8 mm per hour, 50.8 to 127 mm per hour and greater than 127 mm per hour, the shades repeat themselves; grey, white and black. Figure 10 shows an example of the Nimbus 5 ESMR imagery and VIP as displayed on the PPI scope on 15 February 1973. An area of heavy rain is shown east of Miami with rainfall rates between 50.8 to 127 mm per hour.

Each range circle on the scope represents 25 miles and the rain cells recorded by the Miami radar occurred within three minutes of Nimbus 5 overflight.

In order to correlate rainfall rate vs ESMR T_B values, the T_B data were plotted by hand on a 1:3.168 million Mercator map of the Florida region.

Because of a gridding error of approximately 1° latitude along the sub-orbital forward vector of the spacecraft caused by the distortion of the antenna due to solar heating, the T_B analysis had to be fitted to the Florida coastline and Lake Okeechobee, using the warm T_B coastline gradient as a guide. The VIP radar image display was then superimposed on the T_B analysis and a point by point comparison was made. Since the instantaneous field of view for each beam position varied with different nadir angles and sometimes resolved more than one rainfall intensity, the different rainfall intensity elements that fell within the instantaneous field of view were weighted in accordance to areal extent. Only rain elements that fell within a range of 25 miles to 125 miles over the ocean were considered. Figure 11 shows an example of a VIP radar image superimposed upon the ESMR T_B analysis for 1620 GMT on 15 February 1973. It is seen that the location of warm T_B gradients detected by ESMR agree quite well with rain intensity gradients. However, the T_B values within the rain areas which included the high radiances emitted by land (Grand Bahamas Island) were not used in the statistics. In this analysis, 12 case studies were used in which surface wind speeds in the area of the radar images were less than 7 meters per sec and the atmosphere was considered to be sub-tropical maritime. Calculations by Nordberg, et al., 1971, showed that when sea surface winds were less than 7 meters per sec, no changes in microwave brightness temperatures were noted. When sea surface winds were above 7 meters per second, a linear relationship between T_B and surface winds were noted, if atmospheric conditions were kept constant. For example, with sea surface winds of 20 meters per second, an additional increase of 15°K to the sea surface microwave brightness temperature was recorded by aircraft instruments.

The results of the study are shown in Figure 12. The T_B values that fell within the four rain intensity categories are displayed at the mean of each category. For each category the mean T_B and its standard deviation is shown by the solid and dashed lines respectively and listed in Table 1.

Table 1

	Category			
	I	II	III	IV
Mean Rainfall Rate (mm per hr)	1.3	7.6	19.0	38.1
Mean T_B ($^\circ\text{K}$)	185 K	203 K	217 K	227 K
Standard Deviation	10 K	11 K	14 K	9 K

Since there were only nine cases of moderate to heavy rainfall rates in excess of 12.7 mm per hr, the results in Category III and IV are statistically less significant.

In order to verify these empirical results, theoretical calculations of T_B vs rainfall rate were derived from a numerical model devised by Gaut and Reifenstein, 1973. The numerical model solves the equation of radiative transfer at points along the line of sight from a satellite looking toward the Earth in the 19.35 GHz spectral region through a mean sub-tropical maritime atmosphere that contains precipitation at various rainfall rates. The model contains 30 layers 1 km thick from the surface to 30 km, in which the temperature, pressure, density, water vapor and molecular oxygen for the layer are determined from the mean of the parameter in each kilometer layer. The rain model contains one layer in which a uniform Marshall-Palmer droplet distribution is assumed for given rainfall rates from the surface to the freezing level at 4 km. The temperature of the liquid water droplets is 273 K and is isothermal throughout the layer. A "calm" ocean surface is used in the model which assumes a smooth surface for which reflectivity can be calculated using the Fresnel equations for either horizontally or vertically polarized radiation.

The cross sections used in this calculation were the sum of the scattering and absorption coefficients so that the rain effect is certainly overestimated at the higher rain rates. The results of the theoretical calculations are shown in the dashed curve in Figure 13. The theoretical curve is almost linear up to 12 mm per hr and then becomes asymptotic to the 273 K. This indicates that for rainfall rates >18 mm per hr, the microwave energy detected by the Nimbus 5 ESMR will be emitted predominantly from the top of the rain column near the freezing level. The empirically derived data in Figure 13 diverges from the theoretical calculations at the T_B value of 190 K. The reasons for the approximate 20 to 50 K negative difference are:

1. The rain element detected by radar over the "cold ocean" background may not fill the instantaneous field of view of the radiometer, especially in the heavier convective frontal showers and thunderstorms detected within 100 miles of Miami.
2. The approximation for the scattering effect used in the theoretical model.

For lighter, more continuous rainfall occurring over a larger area of stratiform clouds which fill the field of view of the radiometer, the ESMR rainfall rates and the theoretical calculations are in good agreement. Studies are now in progress (Rao and Theon, 1973) to attempt to estimate the latent heat of condensation

released into the atmosphere by utilizing ESMR blackbody temperatures over oceanic rain areas. This term is extremely important in understanding the global heat budget and is an essential input for numerical modeling of the atmosphere.

HYDROLOGICAL AND OTHER APPLICATIONS

The photofacsimile microwave images recorded by Nimbus 5 ESMR indicated a persistent soil moisture feature over the lower Mississippi Valley almost from the first day of launch in December 1972. Abnormally heavy precipitation occurred in October, November, and December 1972, leaving the alluvial Mississippi Valley soils soaked with standing and sub-surface water. Wet soils radiate as "cold" surfaces in the microwave imagery, as shown as white ground areas in Figure 6a. A grid print map analysis was made for this area and is shown in Figure 14. Note that there are two major areas of T_B values < 220 K in the Mississippi Valley which lie within a larger T_B , 240 K envelope. This area was noted to overlay outwash aquifers in the valley drainage field, shown in Figure 15 (National Atlas of the U.S., 1970). A more complete study of the changes of these interesting hydrological features prior to the disastrous Mississippi River flood was made by Schmugge, et al., 1974.

Another surface pattern verification of this feature is shown in the U.S. Air Force DAPP satellite IR imagery which detected the same saturated soil area at 1205 GMT (0605 CST) on December 17, 1972 (Figure 16). The same wet soil feature appeared "warmer" in the 8-13 μm channel. However, at approximately noon on January 22, 1973 the Nimbus 5 THIR (11 μm channel) showed no indication of this region (Figure 17). This was probably due to solar heating which erased the nocturnal differences in surface temperatures that were present just after sunrise.

An analysis was made of the ESMR data (orbit 568), January 22, 1973 over the Gulf Stream in the North Atlantic Ocean, just south of Nova Scotia, under clear daytime sky conditions. Ship observations of sea surface temperature in this shipping lane varied from 8° to 19°C through the Stream. However, there were no indications of this sea surface temperature change found in the ESMR data which was approximately 140 K. Based upon the theoretical data from Lane and Saxton, 1952, the optimum microwave radiometric sensitivity to sea surface temperature was determined to be near the 5 cm wavelength (Figure 18). This factor does explain the insensitivity of ESMR to the Gulf Stream gradients described above.

Future polar orbiting satellites such as the Nimbus F (1974), and G (1978) will utilize different microwave frequencies which will be used to measure the meteorological, oceanographic, and hydrological parameters shown in Figure 19.

THE NIMBUS 5 TEMPERATURE-HUMIDITY INFRARED RADIOMETER (THIR) EXPERIMENT AND DATA ANALYSIS

The THIR flown on Nimbus 5 is a scanning bolometer which is similar to the one flown on Nimbus 4 (McCulloch, 1972). It contains two channels: a 10.5-12.7 μm "window" channel that provided night and day cloud top or surface temperatures with a ground resolution of 4 n. miles (7.7 km) and a 6.5-7.2 μm water vapor absorption channel which peaks at 6.9 μm and senses the integrated moisture content of the upper atmosphere from 250 mb (10.5 km) to 500 mb (5.5 km) with a ground resolution of 13 n. miles (22.6 km) at the sub-satellite point.

Figure 20 shows the photofacsimile imagery for orbit 569, 22 January 1973 for both the 6.7 μm and ESMR data. The moisture rich or cloudy regions are indicated by the white or light grey shading on the 6.7 μm imagery while the drier areas are delineated by the dark grey or black tones.

The ESMR data shows cloud droplet and/or rainfall over water as a warmer brightness temperature (darker grey to black) over a white (cold) background in this 190 K to 260 K range. Heavy clouds or rain occurring over land are better shown in the 250 to 290 K grey scale range. In Figure 21, the 6.7 μm and 11 μm photofacsimile film strips of orbit 570 show some striking differences and similarities. The east-west oriented cirrus clouds relating to the sub-tropical jet stream and scattered heavy cloud masses in the lower half of the pictures appear in both channels. However, the dark cyclonic streaks appearing in the upper half of the 6.7 μm strip do not appear in the 11 μm strip. Since the weighting function of the 6.7 μm channel peaks at 350 mb, a 300 mb chart at 00 GMT for 23 January 1973 was analyzed (Figure 22). Note the strong ridge over the western U.S. and deep trough extending NE/SW from the Great Lakes to Arizona-New Mexico. Superimposed upon this constant pressure height field is the location (grey tone) of the polar jet stream (90 to 110 kts) descending on the west side of the trough and the broad sub-tropical jet stream (110 to 130 kts) ascending along the east side of the trough.

Figure 23 shows the 1:2.5 million Mercator digital grid print map of the 6.7 μm data for orbit 569. The non-zip toned regions (brightness temperatures < 240 K) are areas of high clouds (light grey to white) and the cross-hatched-dotted areas are drier-cloud free zones ($T_B > 240$ K) (dark grey-black) in Figure 21. Figure 24 shows the NMC 650 mb level vertical velocity chart for 1200 GMT, 22 January 1973 which indicates broad areas of downward motion in the north side of the sub-tropical jet oriented NE/SW through Baja California and the Gulf states and along the eastern edge of the polar jet moving southwestward and descending over the Rocky Mountains. Previous studies by Martin and Salomonson (1970) over the U.S. have also related the warmer brightness values (darker areas along the northern edge of the sub-tropical jet) to areas of subsidence. Rodgers, et al.,

(1973) have also described a synoptic situation in which areas of widespread and strong subsidence and advected areas of dry air correspond to areas delineated by high brightness temperatures in Nimbus 3 $6.7\text{ }\mu\text{m}$ MRIR data. An additional parameter that is apparent is that wind direction at the 300 mb level (Figure 22) is easily seen in the cyclonic pattern in this drier area of $6.7\text{ }\mu\text{m}$ data ($> 240\text{ K}$) which outlines the edge of the two major jet streams (Figure 23). Anticyclonic wind flow is also indicated southeast of Florida and Cuba in the $6.7\text{ }\mu\text{m}$ data which was confirmed in the 00 GMT NMC 300 mb Northern Hemisphere charts for 23 January 1973. A qualitative comparison of the moisture patterns on the Nimbus 4 imagery with the 400-mb level conventionally measured wind field had also indicated that the moisture patterns under near clear sky conditions aloft were generally aligned with the wind-field (Allison, et al., 1972). The use of the $6.7\text{ }\mu\text{m}$ observations to improve mid-tropospheric wind flow analyses on a global scale has been discussed by Steranka, et al., 1973, and further research applying the Nimbus 5 THIR $6.7\text{ }\mu\text{m}$ data to the Goddard Institute for Space Studies (GISS) Numerical Model is now in process (Somerville, 1973).

THE NIMBUS 5 VERTICAL TEMPERATURE SOUNDERS AND DATA ANALYSIS

The Nimbus 5 carried aloft three experiments which measured radiances needed to calculate the vertical temperature distribution of the atmosphere from the Earth's surface to the stratosphere, i.e., the Infrared Temperature Profile Radiometer (ITPR), the Nimbus E Microwave Spectrometer (NEMS), and the Selective Chopper Radiometer (SCR). The ITPR contained four channels in the $15\text{ }\mu\text{m}$ carbon dioxide band, one channel in the $19\text{ }\mu\text{m}$ rotational water vapor band, one in the $11\text{ }\mu\text{m}$ "atmospheric window" and one in the $3.8\text{ }\mu\text{m}$ "window". The instrument was designed to derive the temperature profile from the surface to 25 km with a vertical resolution of 3 to 5 km and an estimated accuracy of 2°C .

The SCR had four optical filters and each filter contained four channels for a total of 16 channels whose range of measurement was from $2.06\text{ }\mu\text{m}$ to $133\text{ }\mu\text{m}$. These channels permitted the SCR to extend a temperature sounding up to 45 km with a 3 to 7 km vertical resolution and an estimated accuracy of 2°C .

The NEMS contained five channels, three tuned to the oxygen lines, near 60 GHz, one tuned to the 22 GHz water vapor line, and one tuned to the atmospheric window at 31 GHz. The NEMS provided a $192 \times 192\text{ km}$ surface spatial resolution at nadir while the ITPR and SCR provided 35 km and 43 km instantaneous ground resolutions respectively. The NEMS can sense atmospheric radiances even in the presence of clouds while the ITPR and SCR are strongly affected by clouds within their field of view (ERTS/Nimbus Project, 1972, GARP Project, 1973). Figure 25 shows the weighting functions of each of the various channels of the three vertical temperature sounding systems (Smith, et al., 1973). Selected

examples of the data amalgamation of these three systems during orbit 569, (1638 to 1651 GMT) for 22 January 1973 are shown in Figure 26. These sounding data were kindly provided by Drs. W. L. Smith and N. Grody, NESS, NOAA. The ten temperature profiles were taken in regions of variable relative humidity and cloudiness along the Nimbus 5 sub-satellite track from the sub-tropics to the Arctic Circle (Figure 27). Radiosonde data (1200 GMT) from stations near to the satellite track were plotted for comparison.

Table 2 shows the differences between the conventional and satellite-derived temperature by constant pressure level. Note that there are four levels with the following mean temperature differences. 850 mb: $+2.4^{\circ}\text{C}$, 700 mb to 250 mb: -0.5° to -2.8°C , 200 mb to 100 mb: $+0.2^{\circ}$ to $+3.0^{\circ}\text{C}$, 70 mb to 20 mb: -1.7° to -3.1°C . A positive value indicates that the radiosonde air temperatures are warmer than the satellite-derived vertical air temperature. The mean of the layer mean differences from 850 to 20 mb was -0.9°C .

A comparison (Table 3) was made of the 1000 to 500 mb level thickness (meters) which was derived from the NEMS and NMC thickness data along the Nimbus 5 sub-satellite track of orbit 569 (Figure 28). The NEMS and National Meteorological Center (NMC) data were kindly provided by Prof. D. H. Staelin and R. L. Pettyjohn of MIT. The change in sign and magnitude of the thickness difference at 23.43°N , 30.47°N and 61.55°N were due to a change in the algorithm used in the basic computer program used to derive these thicknesses. The negative sign indicates that the NEMS derived thickness is less than the NMC measured thickness. The largest differences appear to be between approximately 40° to 60°N .

CONCLUSION

It has been shown that the Nimbus 5 ESMR and THIR can be used together as a multi-spectral analysis tool. The thermal microwave emission at 1.55 cm as recorded by the ESMR is sufficiently different from the IR and visible region due to radiative transfer characteristics to provide unique and practical applications for meteorology, oceanography, and hydrology.

The utilization of the ITPR, NEMS and SCR data to produce an amalgamated sounding, can produce significantly better profiles than can be achieved individually (Smith, et al., 1973). The incorporation of this data from the improved Nimbus F vertical sounders (1974) into the new high resolution numerical models at the National Meteorological Center and the Goddard Institute for Space Studies is expected to make a positive impact on the 12 to 24 hour forecast problem.

Table 2

Difference (in °C) between related 1200 GMT radiosonde ascents and Nimbus 5 vertical soundings recorded during orbit 569 on January 22, 1973 from 23.3°N to 72.7°N. (+ indicates the radiosonde data is warmer than the satellite data, - indicates the radiosonde data is colder than the satellite data.)

	23.3°N	26.8°N	30.3°N	33.7°N	37.9°N	41.9°N	47.3°N	54.8°N	58.6°N	72.7°N	Mean
1000 mb	+6.0°	—	—	—	—	—	—	—	—	—	—
850 mb	<u>+4.5°</u>	-1.3°	<u>+3.7°</u>	+1.1°	+1.6°	+4.7°	+5.9°	+3.6°	<u>+5.7°</u>	-5.8°	<u>+2.4°</u>
700 mb	-4.4°	-6.1°	-3.4°	-0.6°	<u>+5.9°</u>	<u>+2.0°</u>	<u>+1.0°</u>	-3.6°	<u>+5.7°</u>	-1.1°	-0.5°
500 mb	-2.6°	-4.7°	-5.0°	-3.7°	<u>+0.4°</u>	-5.6°	-1.1°	-6.3°	<u>+2.0°</u>	-0.2°	-2.7°
400 mb	-4.8°	-7.3°	-2.9°	-6.7°	-3.0°	-0.8°	-1.4°	-4.8°	<u>+2.6°</u>	+1.1°	-2.8°
300 mb	-2.9°	-4.7°	-5.2°	-1.3°	-1.4°	<u>+2.4°</u>	-2.9°	-2.7°	-4.2°	<u>+2.4°</u>	-2.1°
250 mb	-1.3°	-0.1°	-3.3°	<u>+5.7°</u>	<u>+0.7°</u>	-1.0°	-3.6°	-2.2°	-7.4°	-0.2°	-1.3°
200 mb	<u>+2.4°</u>	+2.6°	+4.3°	+6.2°	+0.3°	-1.5°	-1.7°	<u>+3.0°</u>	-2.9°	-2.6°	<u>+0.8°</u>
150 mb	<u>+5.3°</u>	+4.6°	+6.1°	+2.8°	+2.1°	+2.1°	+3.2°	+5.5°	<u>+0.1°</u>	-1.8°	<u>+3.0°</u>
100 mb	<u>+2.9°</u>	+1.5°	<u>+0.1°</u>	-2.7°	-4.3°	<u>+2.6°</u>	+0.6°	<u>+1.9°</u>	-1.1°	<u>+0.9°</u>	<u>+0.2°</u>
70 mb	-2.5°	-3.3°	<u>+1.1°</u>	-0.6°	-3.8°	-1.9°	-3.0°	-0.4°	-3.6°	<u>+1.5°</u>	-1.7°
50 mb	-3.8°	<u>+0.2°</u>	—	-1.2°	-1.0°	-1.3°	—	-3.3°	-7.2°	<u>+0.7°</u>	-2.1°
30 mb	-1.5°	-0.9°	—	-1.8°	-3.4°	-3.1°	—	-5.3°	-4.2°	-5.7°	-3.1°
20 mb	<u>+2.7°</u>	<u>+0.5°</u>	—	<u>+0.7°</u>	-4.2°	-1.8°	—	—	-9.5	—	-1.9
											Mean
											-0.9°

ITPR, NEMS, SCR

NEMS, SCR
(OVERCAST SKIES)

ITPR, NEMS, SCR

Table 3

Comparison of Level Thickness (meters)

Latitude	Difference (meters)	Latitude	Difference (meters)	Latitude	Difference (meters)
19.02°N	-7	35.74°N	-40	52.23°N	-69
19.90°N	-2	36.61°N	-48	53.09°N	-70
20.78°N	-4	37.49°N	-51	53.95°N	-78
21.66°N	-4	38.36°N	-48	54.80°N	-63
22.55°N	0	39.23°N	-53	55.65°N	-62
23.43°N	+7	40.11°N	-72	56.50°N	-74
24.31°N	+12	40.98°N	-51	57.35°N	-59
25.19°N	+16	41.85°N	-73	58.19°N	-54
26.07°N	+19	42.72°N	-77	60.71°N	-5
26.95°N	+28	43.59°N	-76	61.55°N	+2
27.83°N	+39	44.46°N	-87	62.38°N	+10
28.71°N	+55	47.06°N	-74	63.20°N	+27
29.59°N	+72	47.93°N	-71	64.03°N	+36
30.47°N	-5	48.79°N	-82	64.85°N	+32
33.11°N	-22	49.65°N	-75	65.66°N	+31
33.98°N	-28	50.51°N	-80	66.47°N	+36
34.86°N	-29	51.37°N	-74	67.27°N	+49

ACKNOWLEDGMENTS

The authors wish to acknowledge the assistance of Major H. Brandli, Det. 11, 6th Weather Wing, Patrick AFB, Florida, in obtaining FPS-77 weather radar data; Mr. Mark Smith for his work in analyzing the WSR-57 radar data; Mr. John Theon, GSFC; and Major Lee Dickenson, Hqtrs., Air Weather Service, USAF; for the use of several figures in this paper.

REFERENCES

- Aerojet ElectroSystems Co., 1973: "Meteorological Applications of Passive Microwave Radiometry," Final Report, SAMSO TR No. 73-206, Vol. III, Part I and II, 1750 FR-1, Azusa, California.
- Allison, L. J., J. Steranka, G. T. Cherrix, E. Hilsenrath, 1972: "Meteorological Applications of the Nimbus 4 Temperature-Humidity Infrared Radiometer, 6.7 μ m Channel Data," Bulletin of the American Meteorological Society, Vol. 53, No. 6, pp. 526-535.
- Battan, L., 1959: "Radar Meteorology," University of Chicago Press, Chicago, Illinois.
- Campbell, W. J., P. Gloersen, W. Nordberg, T. T. Wilheit, 1973: "Dynamics and Morphology of Beaufort Sea Ice Determined from Satellites, Aircraft and Drifting Stations;" Paper A.5.6, (to be published: The Proc. of Symposium on Approaches to Earth Sciences Through the Use of Space Technology), Cospar, Working Group 6, Constance, Germany.
- Catoe, C., W. Nordberg, P. Thaddeus, G. Ling, 1967: "Preliminary Results from Aircraft Flight Tests of an Electrically Scanning Microwave Radiometer," NASA X-622-67-352, Goddard Space Flight Center, Greenbelt, Maryland, 35 pp.
- ERTS/Nimbus Project, 1972: "The Nimbus 5 Users Guide," NASA, Goddard Space Flight Center, Greenbelt, Maryland.
- Follansbee, W., 1973: "Estimation of Average Daily Rainfall from Satellite Cloud Photographs," NOAA Tech. Memo. NESS 44, National Environmental Satellite Service, NOAA, Washington D. C., 39 pp.
- GARP Project, 1973: "GARP Project Data Systems Test Plan," Goddard Space Flight Center, Greenbelt, Maryland.
- Gaut, N. and P. Reifstein III, 1973: Private Correspondence.
- Gloersen, P., W. Nordberg, T. J. Schmugge, T. T. Wilheit, W. J. Campbell, 1972: "Microwave Signatures of First-Year and Multi-Year Sea Ice," NASA X-652-72-312, Goddard Space Flight Center, Greenbelt, Maryland, 19 pp.
- Gloersen, P., T. C. Chang, T. T. Wilheit, W. J. Campbell, 1973(a): "Polar Sea Ice Observations by Means of Microwave Radiometry," NASA X-652-73-341, Goddard Space Flight Center, Greenbelt, Maryland, 10 pp.

- Gloersen, P., W. Nordberg, T. J. Schmugge, T. T. Wilheit, 1973(b): "Microwave Signatures of First Year and Multi-Year Sea Ice," JGR, Vol. 78, No. pp 3564-3572.
- Gloersen, P., T. T. Wilheit, T. C. Chang, W. Nordberg and W. J. Campbell, 1973(c): "Microwave Maps of the Polar Ice of the North," NASA X-652-73-269, Goddard Space Flight Center, Greenbelt, Maryland.
- Gunn, K. L. S. and T. U. R. East, 1954: "The Microwave Properties of Precipitation Particles," Quart, J. Met. Soc., 80, 522-545.
- Hollinger, J. P., 1971: "Passive Microwave Measurements of Sea Surface Roughness," IEEE, Trans. on Geoscience Electronics, GE-9, No. 3, 165-169.
- Lane, J. A. and J. A. Saxton, 1952: "Dielectric Dispersion in Pure Polar Liquids at Very High Radio-Frequencies," Proc. Roy. Soc. A214: 400-545.
- Leighton, R. B., 1959: "Principles of Modern Physics," McGraw-Hill Book Co., New York, New York.
- Martin, F. L. and V. V. Salomonson, 1970: "Statistical Characteristics of Subtropical Jet Stream in Terms of MRIR Observations from Nimbus 2," J. of Applied Met, 9, No. 3, 508-520.
- Martin, D. W. and W. D. Scherer, 1973: "Review of Satellite Rainfall Estimation Methods," Bulletin of the American Meteorological Society, Vol. 54, No. 7, 661-674.
- McCulloch, A. W., 1972: "The Temperature-Humidity Infrared Radiometer (THIR) Subsystem," Nimbus 5 Users Guide, NASA, Goddard Space Flight Center, Greenbelt, Maryland, 11-47.
- National Atlas of the United States of America, 1970: United States Department of the Interior, Geological Survey, Washington, D. C.
- Nordberg, W., J. Conaway and P. Thaddeus, 1969: "Microwave Observations of Sea State from Aircraft," Quart. J. Roy. Meteorological Society, 95, 408.
- Nordberg, W., J. W. Conaway, D. B. Ross and T. Wilheit, 1971: "Measurement of Microwave Emission from a Foam-Covered Wind Driven Sea," J. Atmos. Sci., 28, No. 3, 429-435.

- Paris, J. F., 1969: "Microwave Radiometry and Its Application to Marine Meteorology and Oceanography," Ref. No. 69-IT, Dept. of Oceanography, Texas A&M University, College Station, Texas.
- Paris, J. F., 1971: "Transfer of Thermal Microwaves in the Atmosphere," II, Dept. of Meteorology, Texas A&M University, College Station, Texas, Contract Final Report, NASA Grant NGR 44-001-098, NASA, GSFC, 211 pp.
- Porter, R. A. and F. J. Wentz, III, 1972: "Research to Develop a Microwave Radiometric Ocean Temperature Sensing Technique," Final Report, Vol. 1, 2, Radiometric Technology Inc. Wakefield, Mass., Contract 2-35309, for USDOC, NOAA, NESS.
- Rao, M. and J. Theon, 1973: Private Correspondence.
- Rodgers, E. B., V. V. Salomonson, and L. Kyle, 1973: "Upper Tropospheric Dynamics as Reflected in the Nimbus 4 THIR $6.7 \mu\text{m}$ Data," NASA TN D-7493, pp 27.
- Ross, D. B., V. T. Cardone, and J. W. Conaway, 1970: "Laser and Microwave Observations of Sea Surface Condition for Fetch-Limited 17 to 25 m/sec Winds," IEEE Trans. on Geoscience Electronics, GE-8, No. 4, 326-336.
- Sabatini, R. R. and E. S. Merritt, 1973: "The Nimbus 5 ESMR and Its Application to Storm Detection," Final Report Contract No. N62306-72-C-0153, Environmental Prediction Research Facility, U. S. Navy, Monterey, California.
- Schmugge, T., P. Gloersen and T. T. Wilheit, 1972: "Remote Sensing of Soil Moisture with Microwave Radiometers," NASA X-652-72-305, Goddard Space Flight Center, Greenbelt, Maryland, 32 pp.
- Schmugge, T., A. Rango, L. J. Allison, and T. Wilheit, 1974: "Hydrologic Applications of Nimbus 5 ESMR Data," NASA X-910-74-51, Goddard Space Flight Center, Greenbelt, Md., pp. 21.
- Skidmore, R. W. and J. F. W. Purdom, 1973: "Application of Meteorological Satellite Data in Analysis and Forecasting," Supplement #2 to ESSA Tech. Report NESC 51, U. S. Department of Commerce, NOAA, NESS, Washington, D. C., 59 pp.

- Smith, W. L., D. H. Staelin and J. T. Houghton, 1973: "Vertical Temperature Profiles from Satellites - Results from Second Generation Instruments Aboard Nimbus 5," presented at the Cospar Symposium on Approaches to Earth Survey Problems Through the Use of Space Techniques, Konstanz, F. R. of Germany, May 23-June 6, 1973.
- Somerville, R., 1973: "The GISS Model of the Global Atmosphere," NASA X-600-73-254, 37-82.
- Steranka, J., L. J. Allison and V. V. Salomonson, 1973: "Application of Nimbus 4 THIR $6.7 \mu\text{m}$ Observations to Regional and Global Moisture and Wind Field Analyses," Journal of Applied Meteorology, Vol. 12, No. 2, pp 386-395.
- Theon, J., 1973: "A Multispectral View of the Gulf of Mexico from Nimbus 5," Bulletin of the American Meteorological Society, Vol. 54, No. 9, pp 934-937.
- U. S. Department of Commerce, 1971: "Satellite Data Requirements of Atlantic Oceanographic and Meteorological Laboratories for Studies of Ocean Physics and Solid Earth," NOAA Technical Report ERL 225-AOML 5, Environmental Research Laboratories, Boulder, Colorado, 46 pp.
- Wilheit, T. T., 1972: "The Electrically Scanning Microwave Radiometer (ESMR) Experiment," Nimbus 5 User's Guide, NASA, Goddard Space Flight Center, Greenbelt, Maryland, 59-105.
- Wilheit, T. T., J. C. Blinn, W. Campbell, A. Edgerton and W. Nordberg, 1972: "Aircraft Measurements of Microwave Emission from Arctic Sea Ice," Remote Sensing of the Environment, Vol. 2, page 129 to 139.
- Wilheit, T. T., J. Theon, W. Shenk, and L. J. Allison, 1973: "Meteorological Interpretations of the Images from Nimbus 5 Electrically Scanned Microwave Radiometer." NASA X-651-73-189, Goddard Space Flight Center, Greenbelt, Maryland, 21 pp.

NIMBUS 5

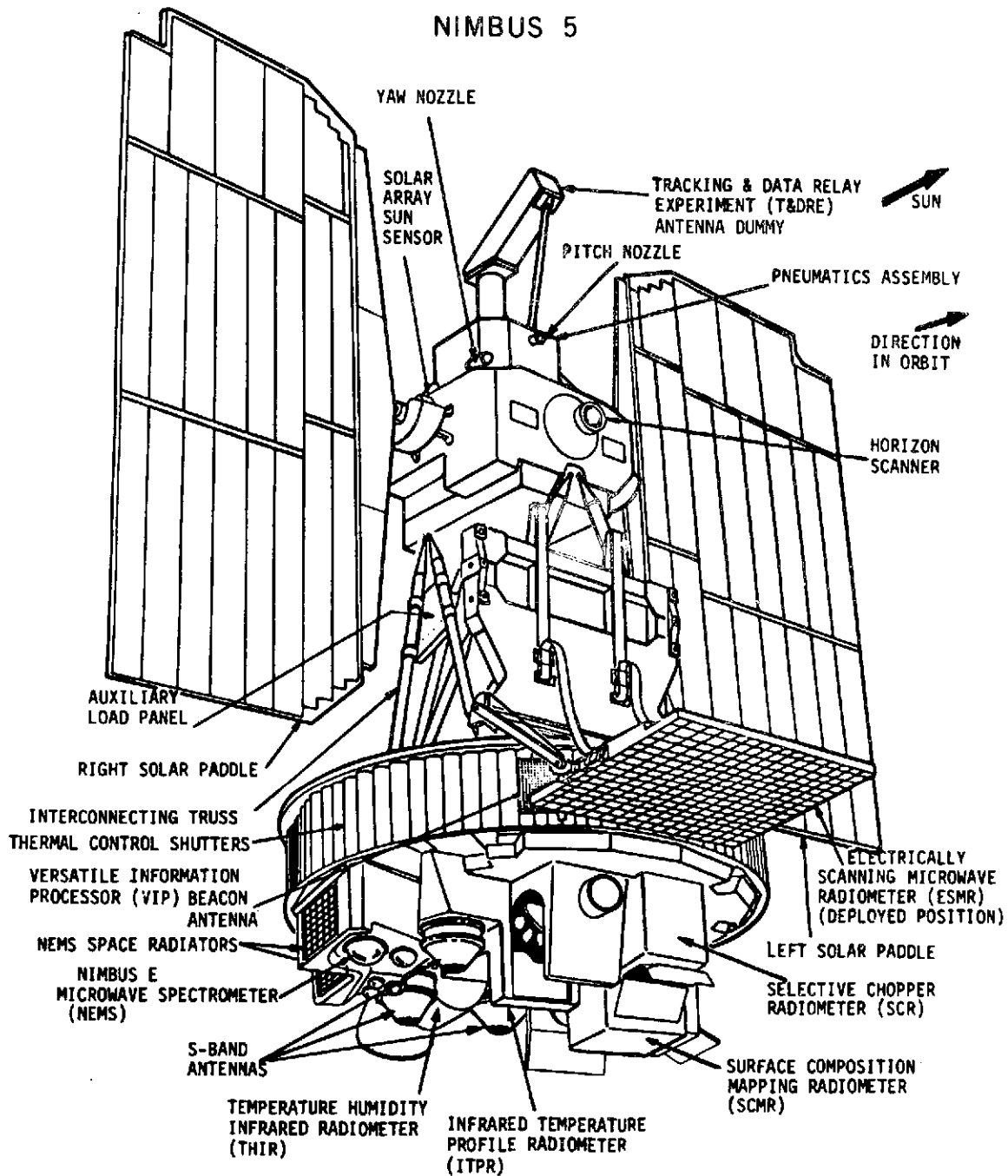


Figure 1. The Nimbus 5 Spacecraft with associated experiments.

BRIGHTNESS

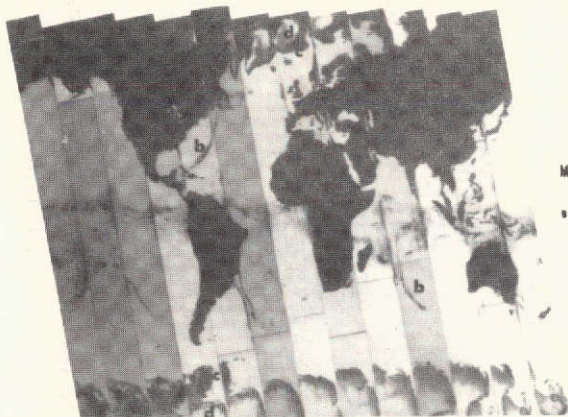
TEMPERATURE

MONTAGES



BRIGHTNESS TEMPERATURE RANGE 130°K to 210°K

MONTAGE 1



MONTAGE 2

BRIGHTNESS TEMPERATURE RANGE

194°K to 266°K

MONTAGE 3

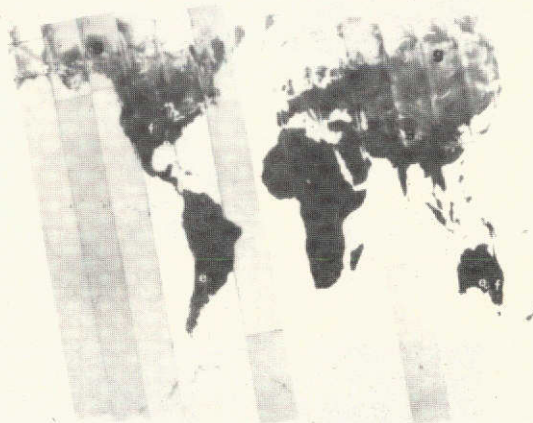
BRIGHTNESS TEMPERATURE RANGE 254°K to 290°K

By dividing the total brightness temperature range of the Electrically Scanning Microwave Radiometer (ESMR) data into three overlapping subranges, various meteorological and hydrological features are easily delineated.

The low brightness temperatures in montage 1 show rainfall areas and variations in atmospheric moisture (a) over oceans, but no information is discernible over the dark land masses.

The medium brightness temperatures in montage 2 indicate areas of intense rainfall (b) over oceans, and show contrasts between first year ice formations (c) and older ice and snow (d).

The high brightness temperatures in montage 3 show areas of high soil moisture (e), heavy rainfall (f), and snow cover (g) over land masses, while ocean areas contain little or no information.



4 FEBRUARY 1973

DAYTIME DATA ORBITS 735 through 747

Figure 2. Nimbus 5 ESMR Photofacsimile Global Montages for February 4, 1973, orbits 735 through 747, 19.35 GHz.

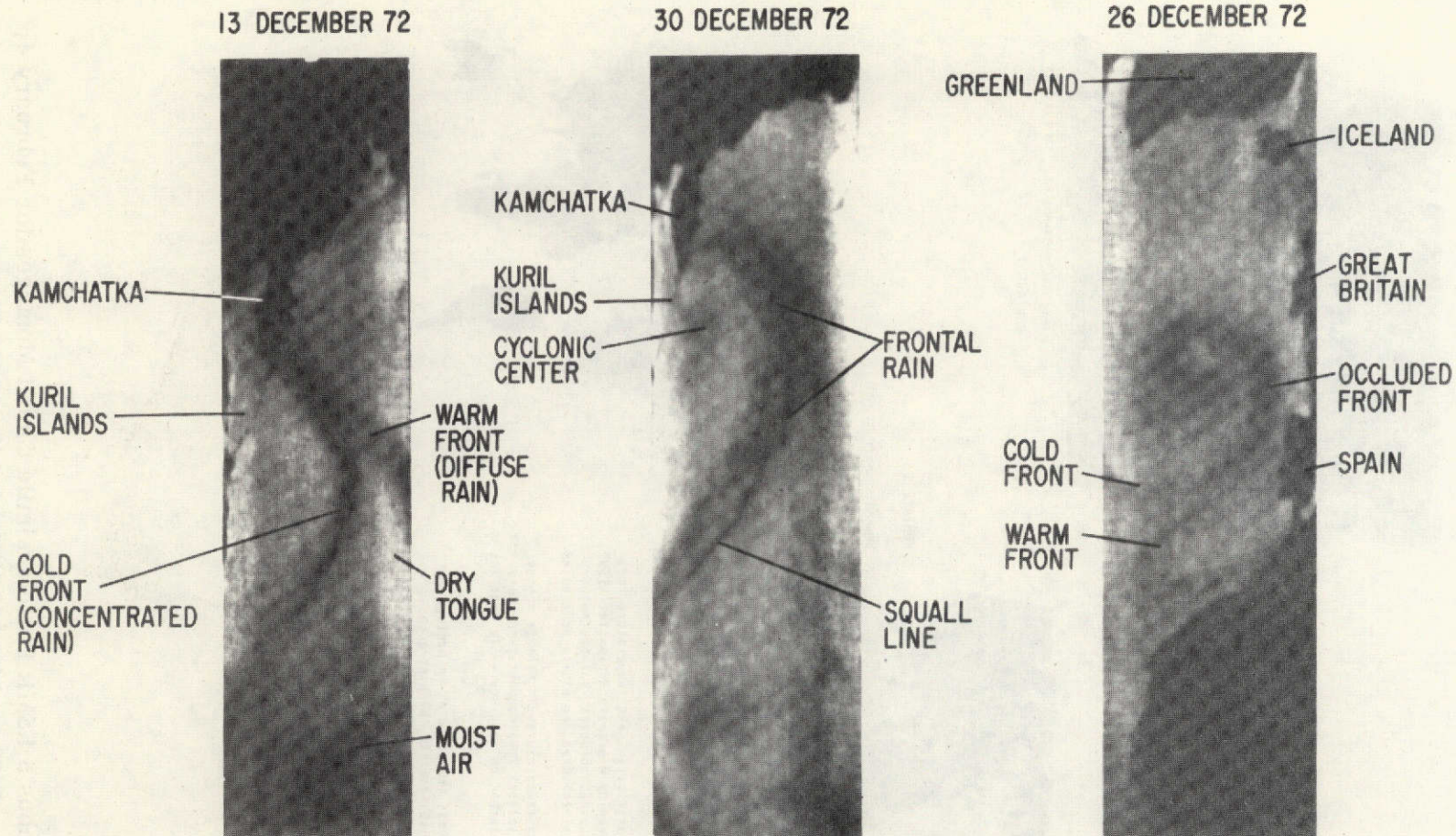
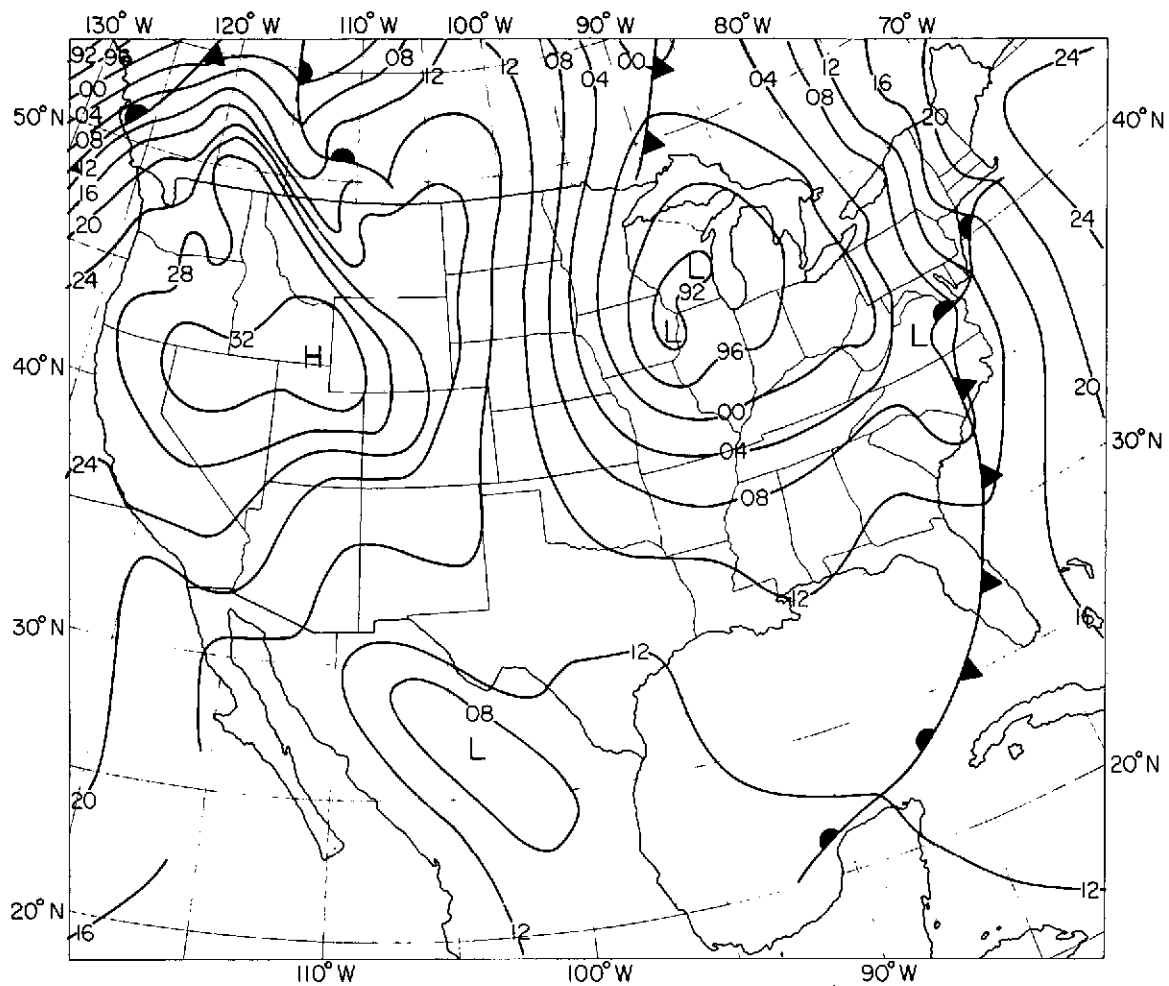


Figure 3. Nimbus 5 ESMR Photofacsimile Images of Mid-Latitude Frontal Systems (T_B range: 190 to 250 K), 19.35 GHz



NATIONAL WEATHER SERVICE
 NORTH AMERICAN SURFACE CHART
 1800 GMT 22 JANUARY 1973

Figure 4. National Meteorological Center, National Weather Service
 North American Surface Chart, 1800 GMT, January 22, 1973.



Figure 5a. U.S. Air Force Data Acquisition and Processing Program (DAPP) image of visual data (0.4 to 1.1 μm , day), 1600-1800 GMT, January 22, 1973 (1/3 n. mi. resolution).

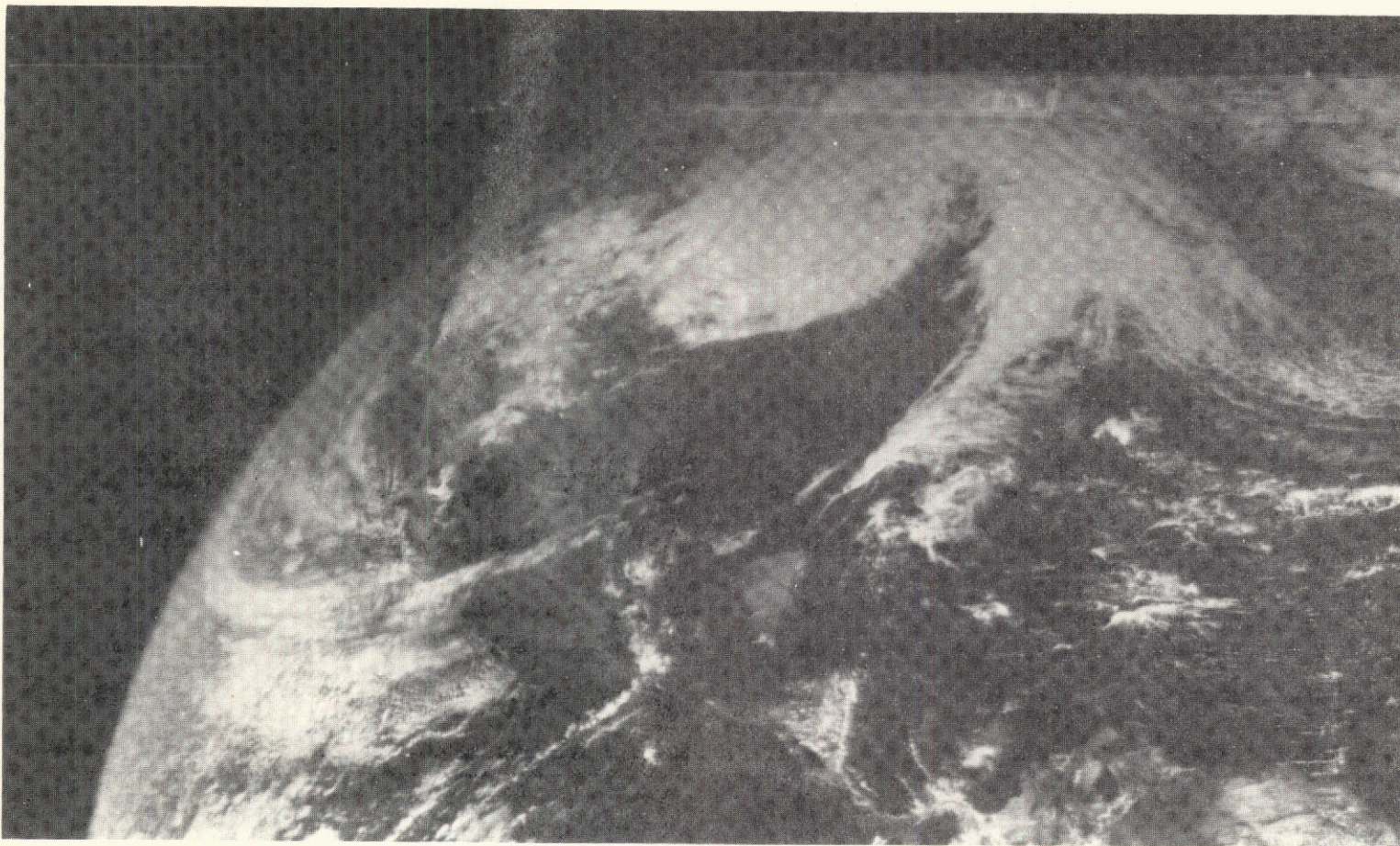


Figure 5b. ATS-3 image recorded at 1704 GMT, January 22, 1973.



Figure 5c. Nimbus 5 THIR Photo-
facsimile image, orbit 569 (day),
January 22, 1973 ($11\ \mu\text{m}$).



Figure 6a. Nimbus 5 ESMR Photofacsimile image, orbit 569 (day)
January 22, 1973, 19.35 GHz

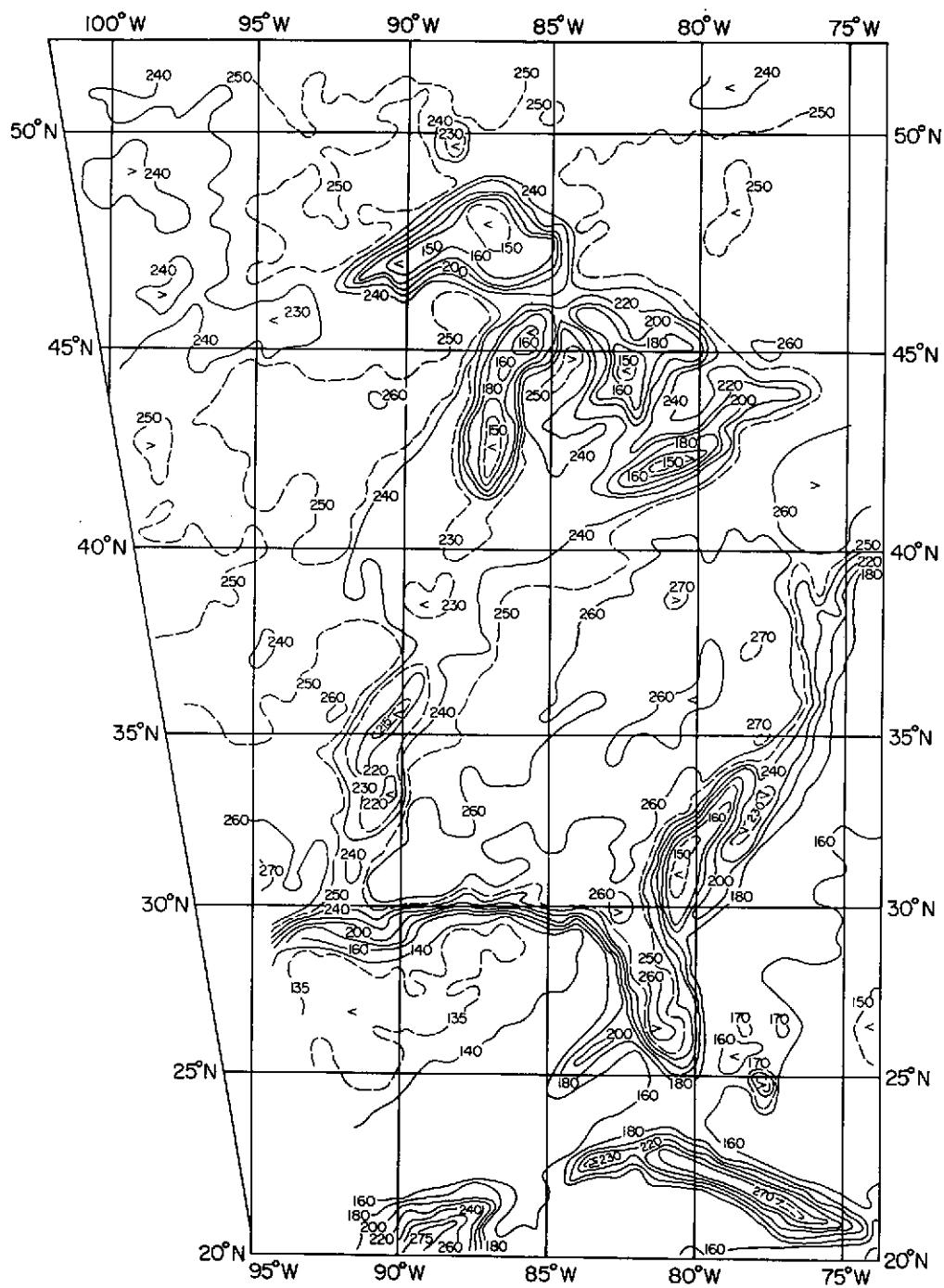


Figure 6b. Nimbus 5 ESMR grid print map analysis T_B in K 1:5
 Million Mercator, 1637 to 1648 GMT, orbit 569,
 January 22, 1973, 19.35 GHz.

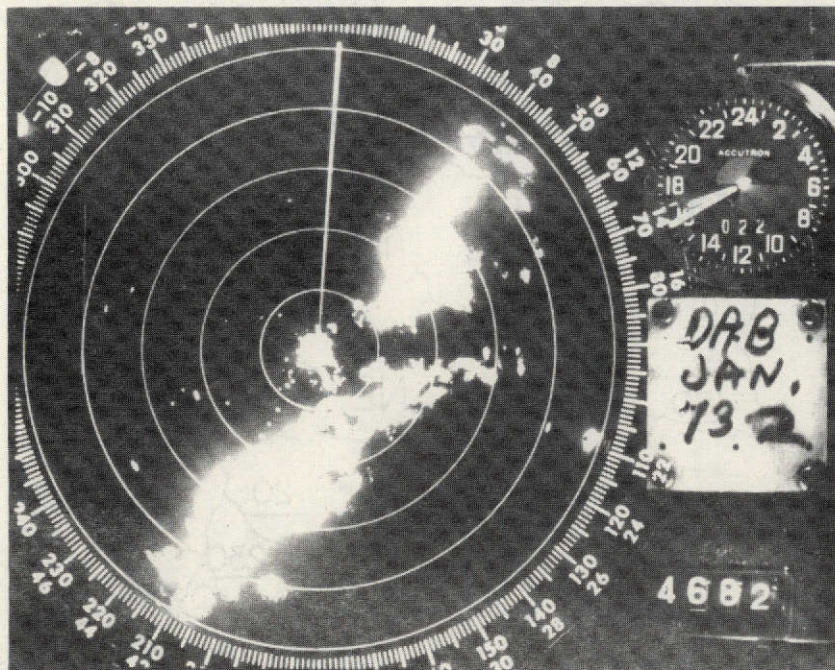


Figure 8a. National Weather Service WSR-57 (10 cm) weather radar PPI polaroid image, recorded 1640 GMT, January 22, 1973 at Daytona Beach, Florida (25 mile range markers).

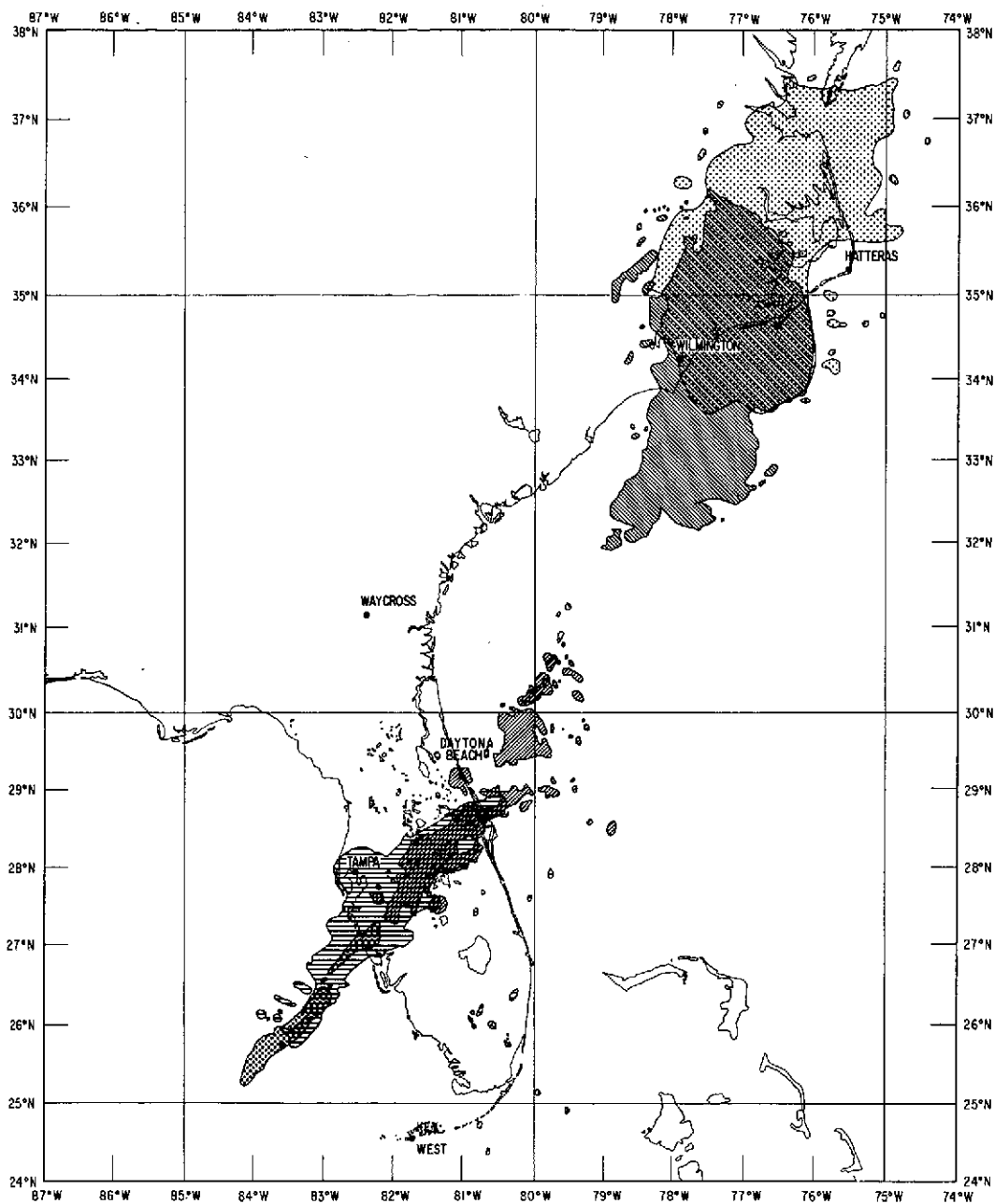


Figure 8b. Hand-rectified National Weather Service WSR-57 weather radar images from Key West, Florida, Tampa, Florida, Daytona Beach, Florida, Waycross, Georgia, Wilmington, North Carolina, Hatteras, North Carolina, from 1637 to 1643 GMT, January 22, 1973. (Darker gray hatching indicates overlapping radar echoes.)

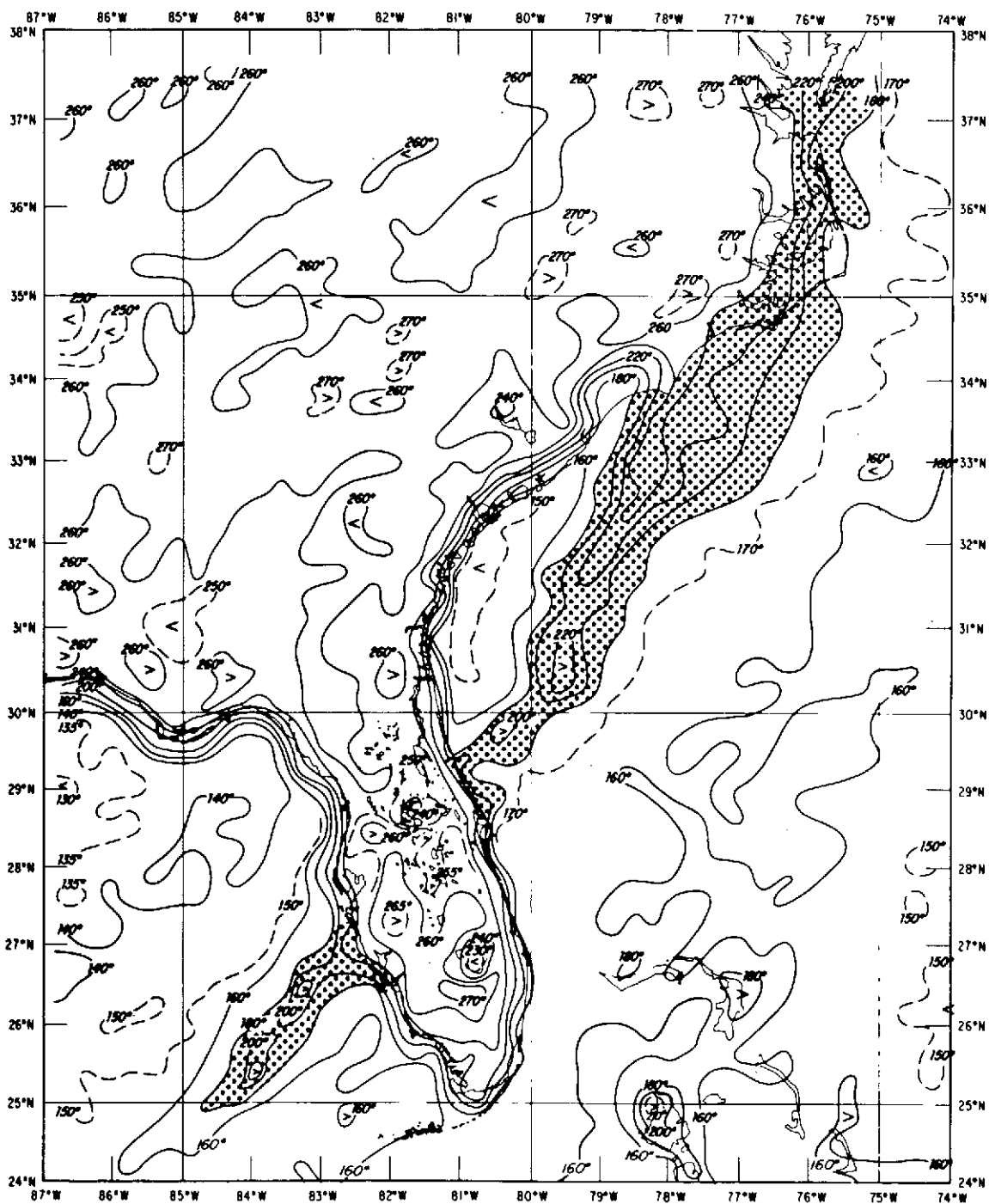


Figure 8c. Nimbus 5 ESMR grid print map analysis. T_B in K, 1:2.5 Million, Mercator, 1639 to 1643 GMT, orbit 569, January 22, 1973, 19.35 GHz.
(Dotted area: $T_B > 180$ K over water.)

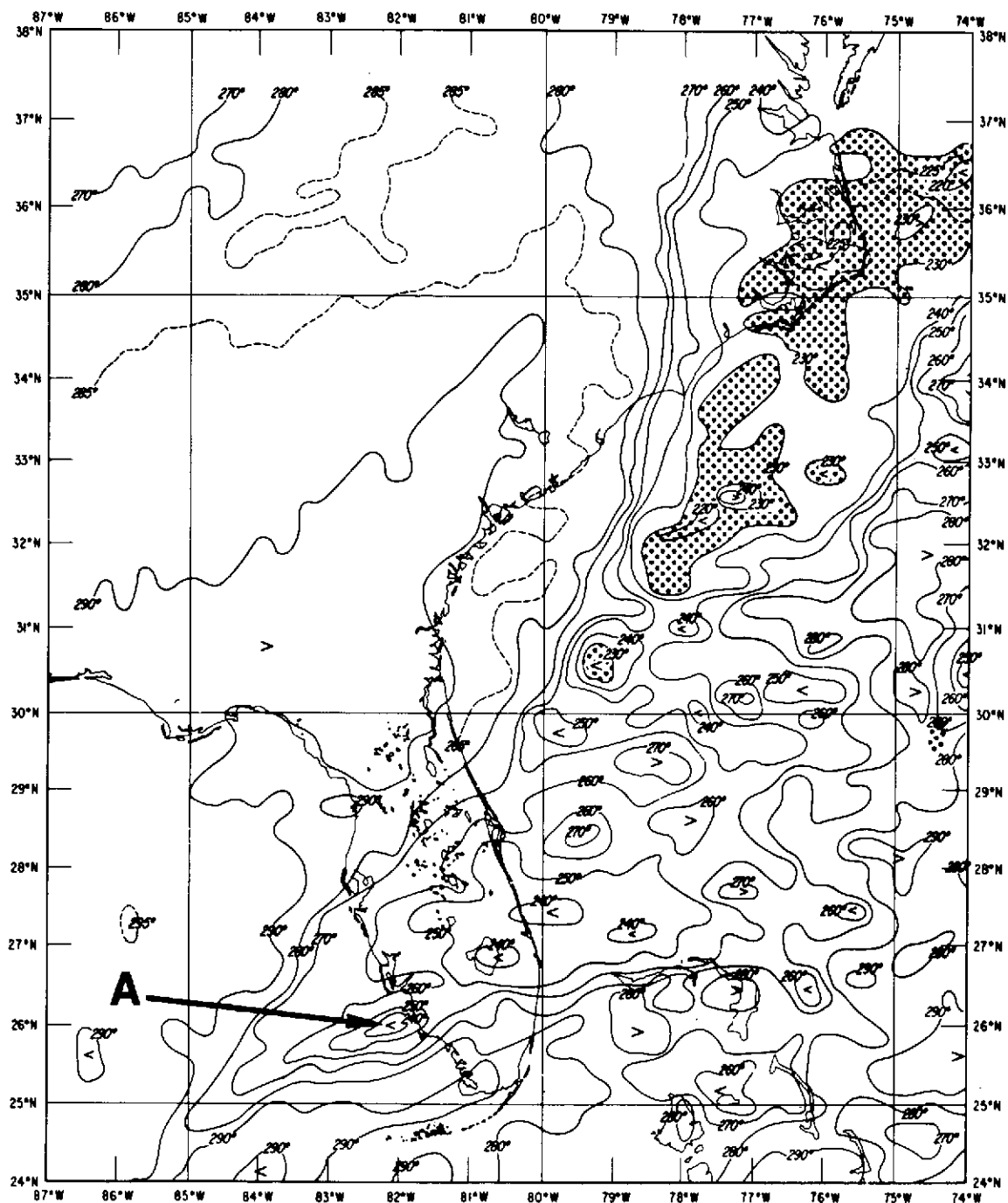


Figure 8d. Nimbus 5 THIR grid print map analysis, T_B in K, 1:2.5 Million, Mercator, 1639 to 1643 GMT, orbit 569, January 22, 1973, $11 \mu\text{m}$. (Dotted area: $T_B < 230 \text{ K}$.) Arrow (A) indicates cirrus cloud blowoff in vicinity of sub-tropical jet stream

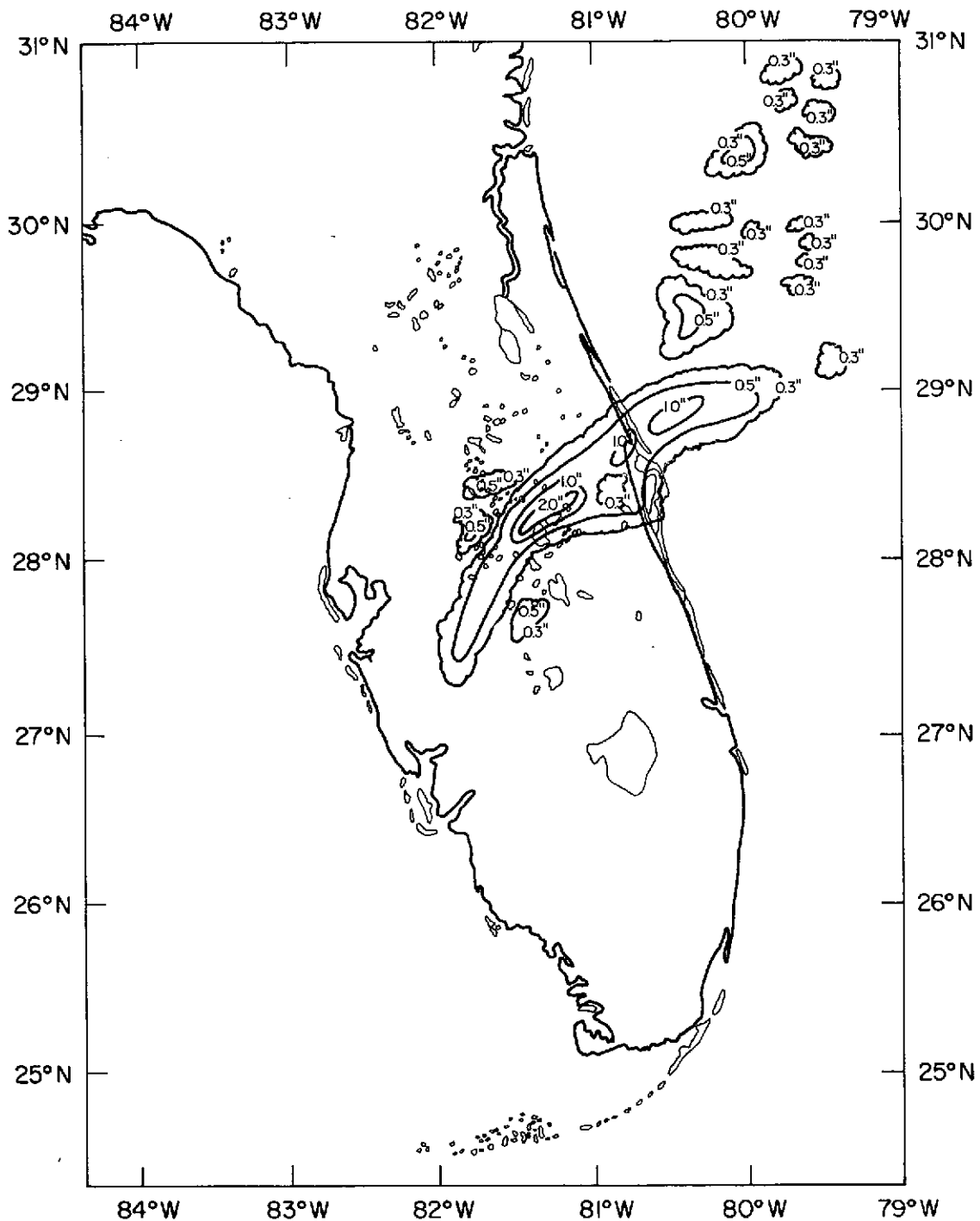


Figure 9a. U.S. Air Force, AWS FPS-77 (5.4 CM), Cape Kennedy, Florida, weather radar analyses, hand-rectified to 1:2.5 Million Mercator map, 1641 GMT, January 22, 1973. (Rainfall rate isolines: 0.3, 0.5, 1 and 2 inches per hour.)

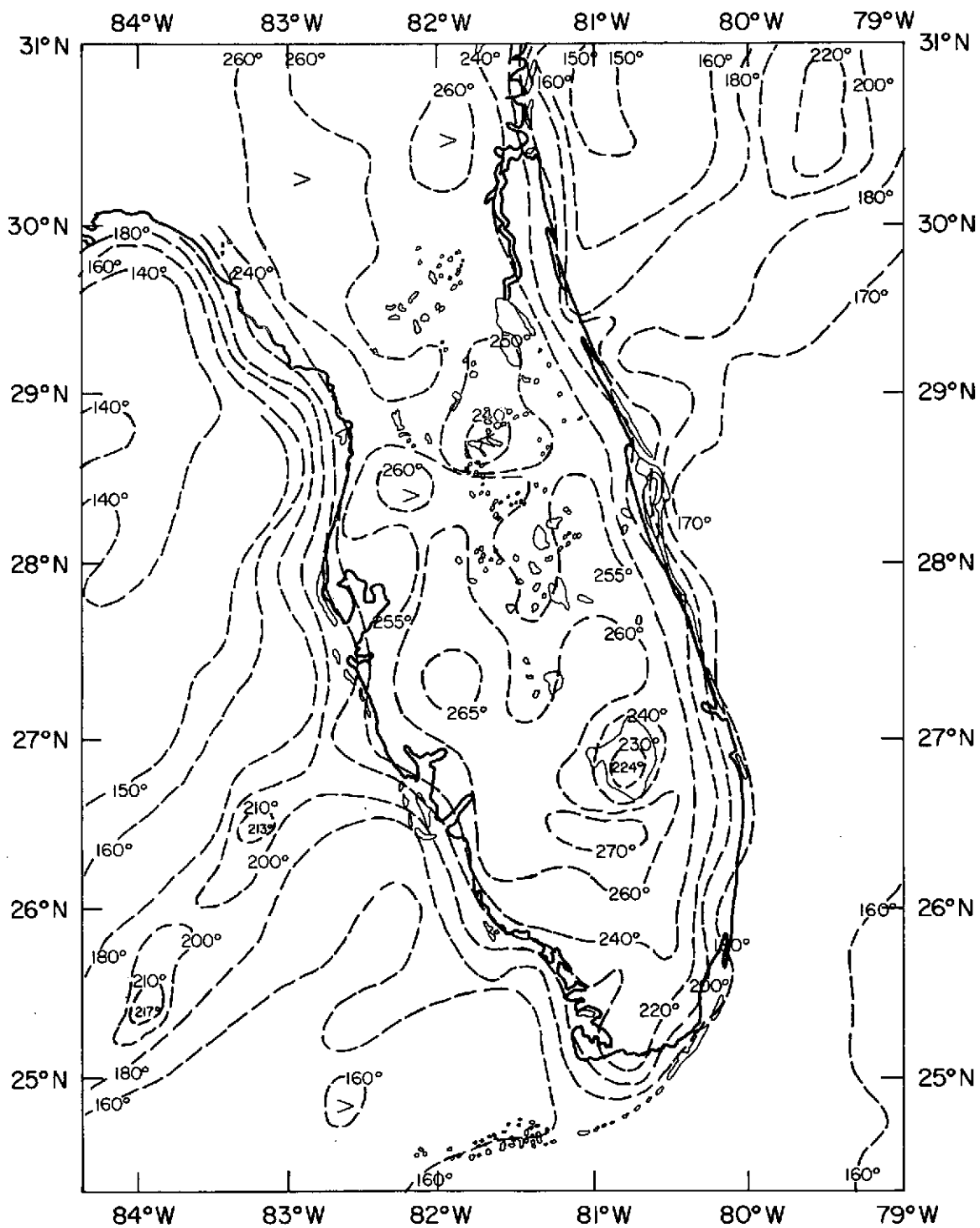


Figure 9b. Nimbus 5 ESMR grid print map analysis, T_B in K,
 1:2.5 Million Mercator, 1638 to 1641 GMT, orbit 569 (day),
 January 22, 1973, 19.35 GHz.

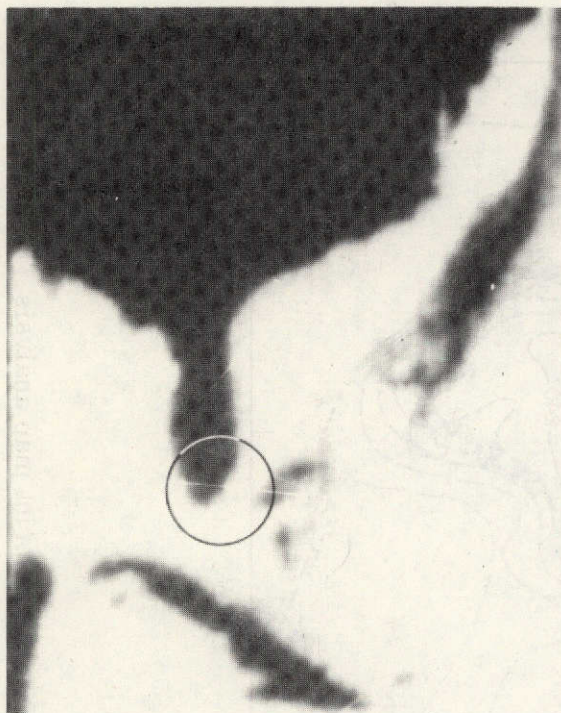


Figure 10a. Nimbus 5 ESMR Photo-facsimile Image, Orbit 891, 1623 GMT, 15 February, 1973.

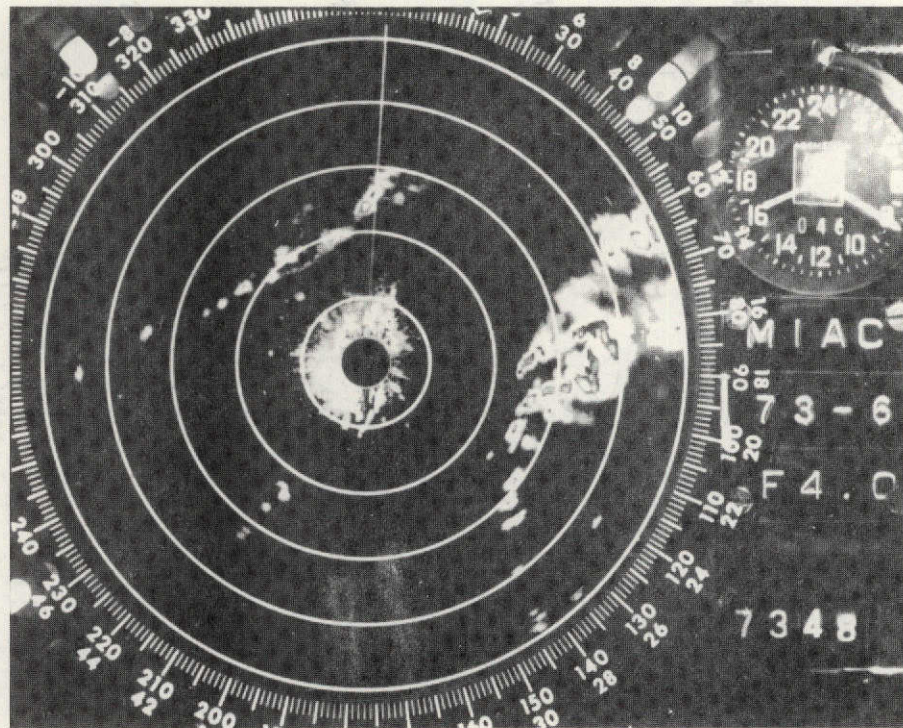


Figure 10b. National Weather Service WSR-57 (10 cm) weather radar PPI polaroid image (VIP), recorded at 1620 GMT, 15 February 1973 (25 mile range markers).

MIAMI RADAR
WSR-57 (VIP)
15 FEBRUARY 1973
1620 GMT

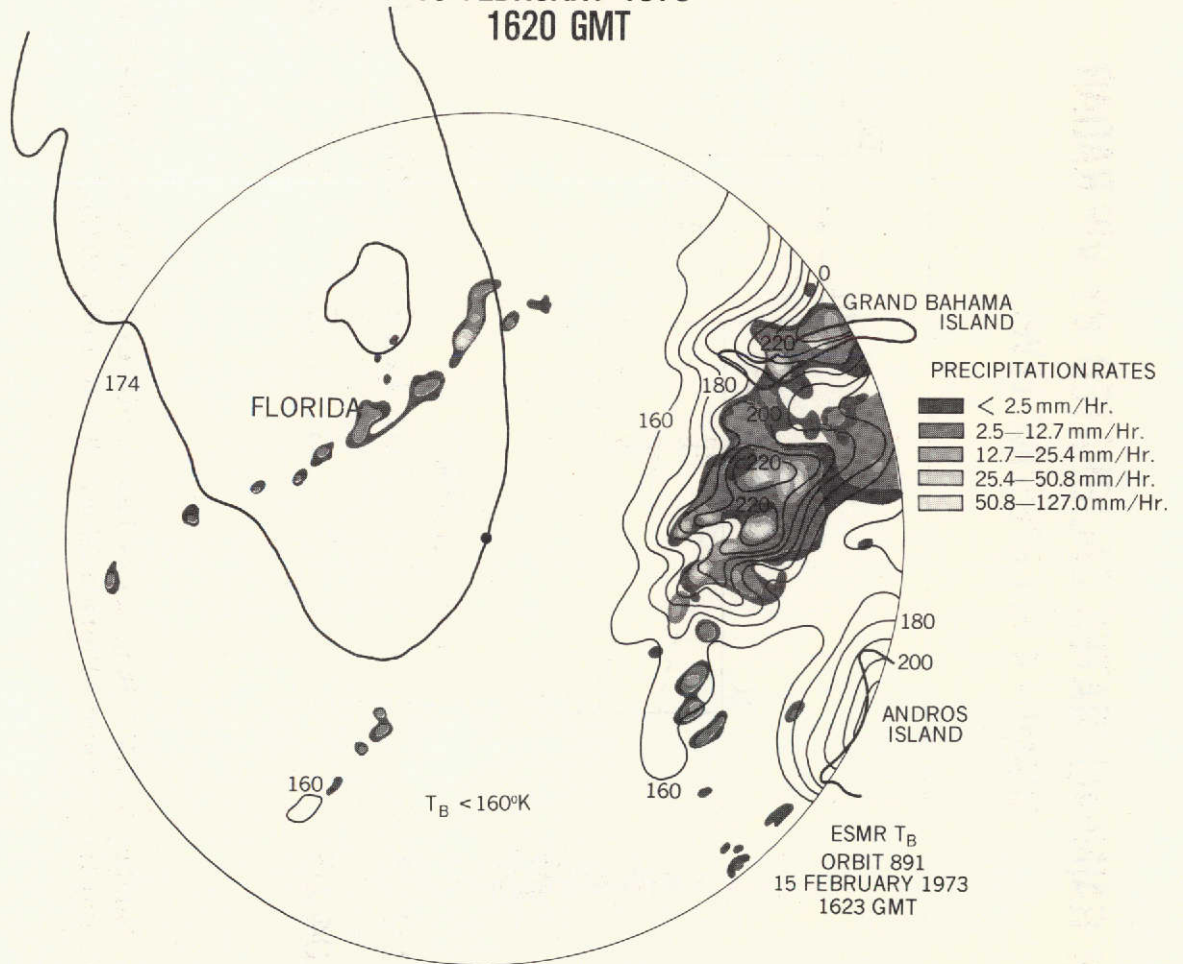


Figure 11. Hand-rectified National Weather Service WSR-57 weather radar image from Miami, Florida superimposed on a T_B analysis of individual Nimbus 5 ESMR scan spots (30° nadir angle limit).

ESMR RAINFALL RATES CALIBRATED BY VIP RADAR

MIAMI - 4 Km FREEZING LEVEL

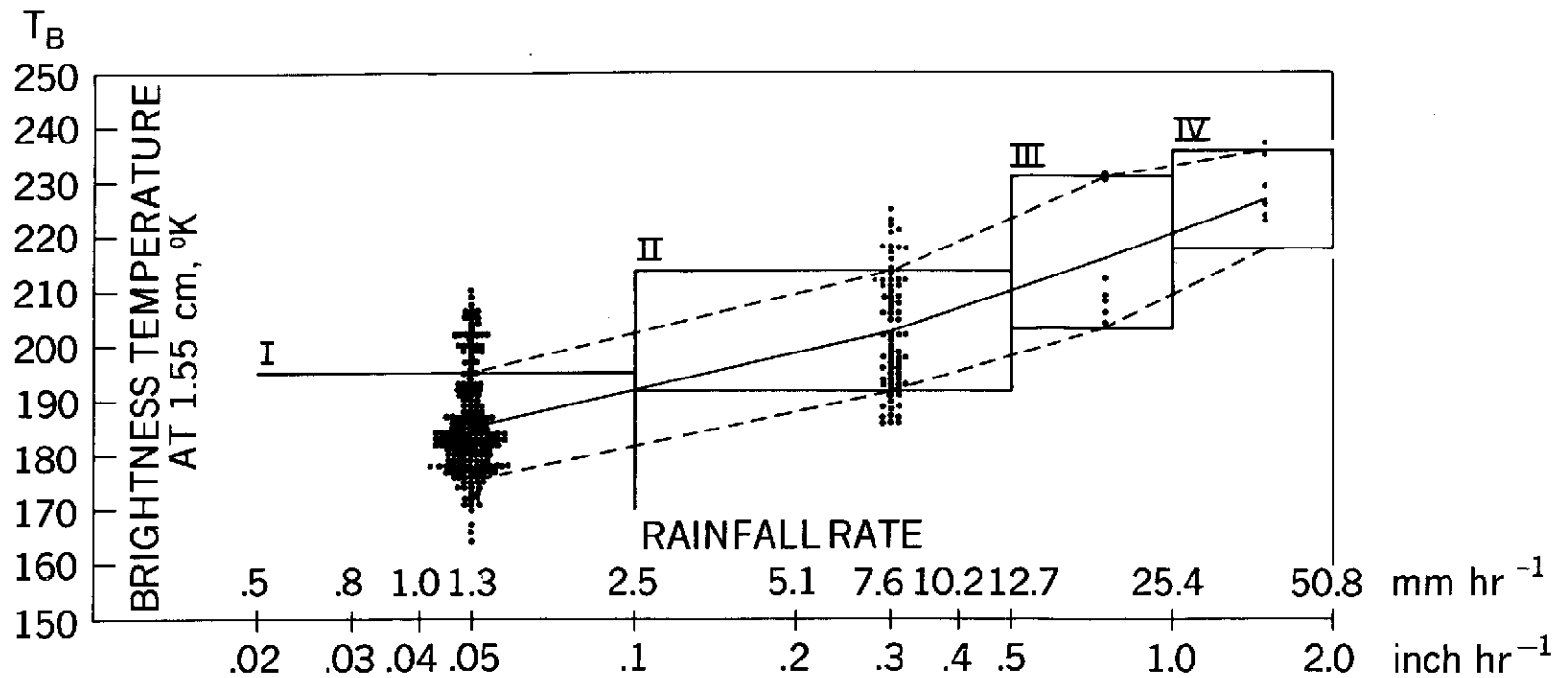


Figure 12. Four categories of Nimbus 5 ESMR Brightness Temperatures (°K) versus WSR-57 Rainfall Rates (VIP data) from Miami, Florida (Dec. 1972 to Feb. 1973).

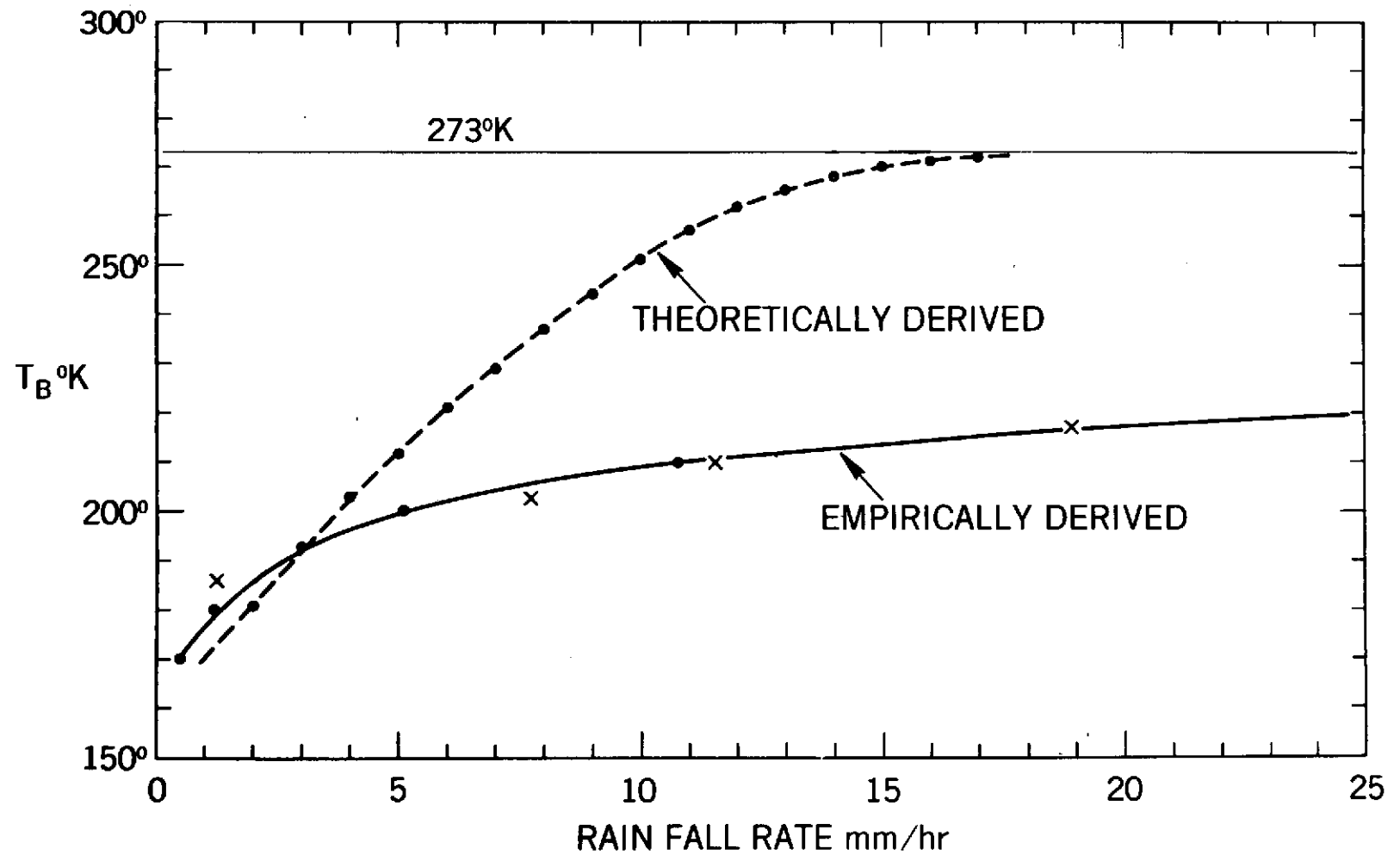


Figure 13. Nimbus 5 ESMR Brightness Temperatures ($^{\circ}$ K) versus Rainfall Rates (mm per hr), empirically derived (Fig. 12) and theoretically derived (after Gaut Reifenstein, 1973).

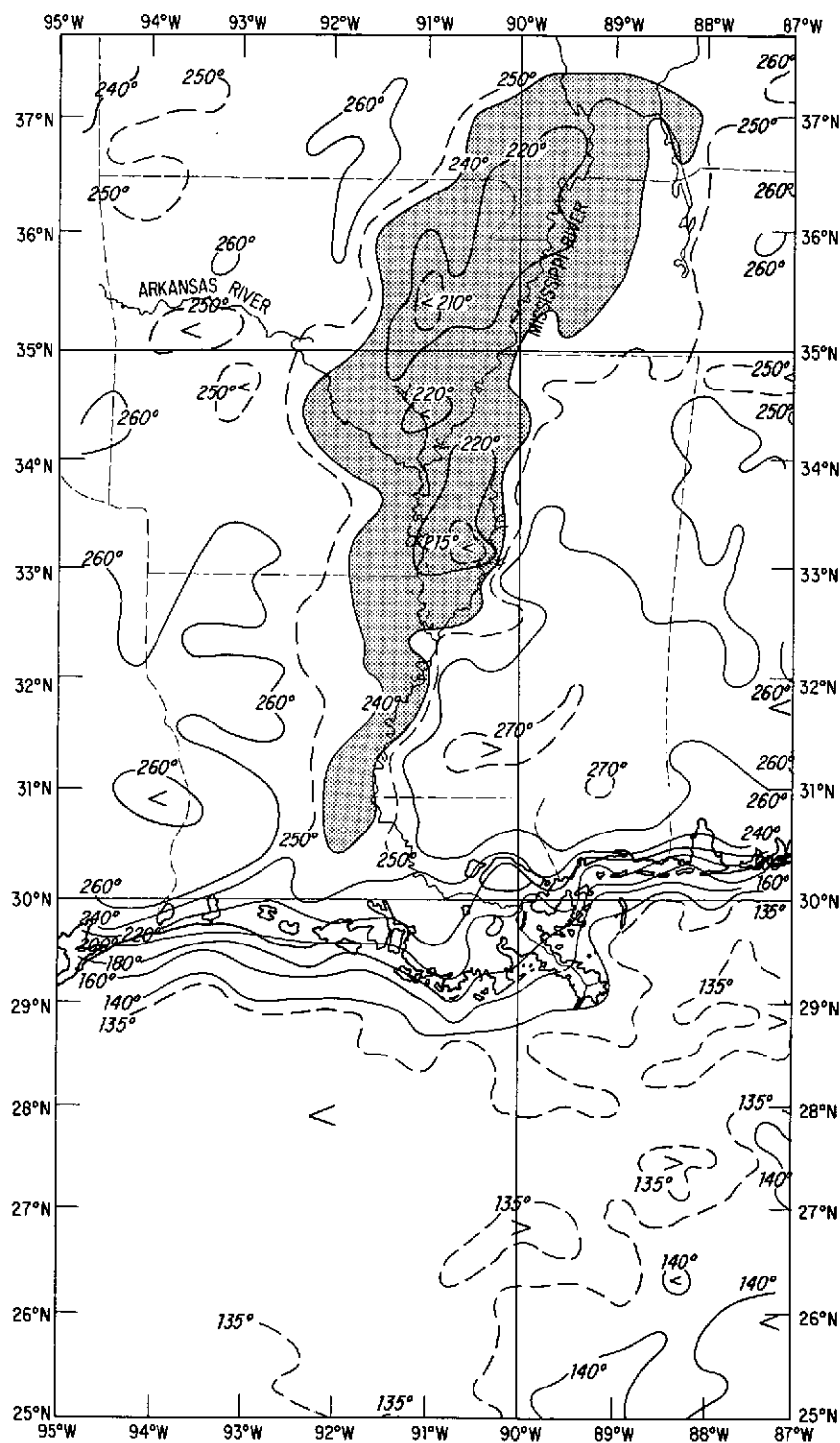
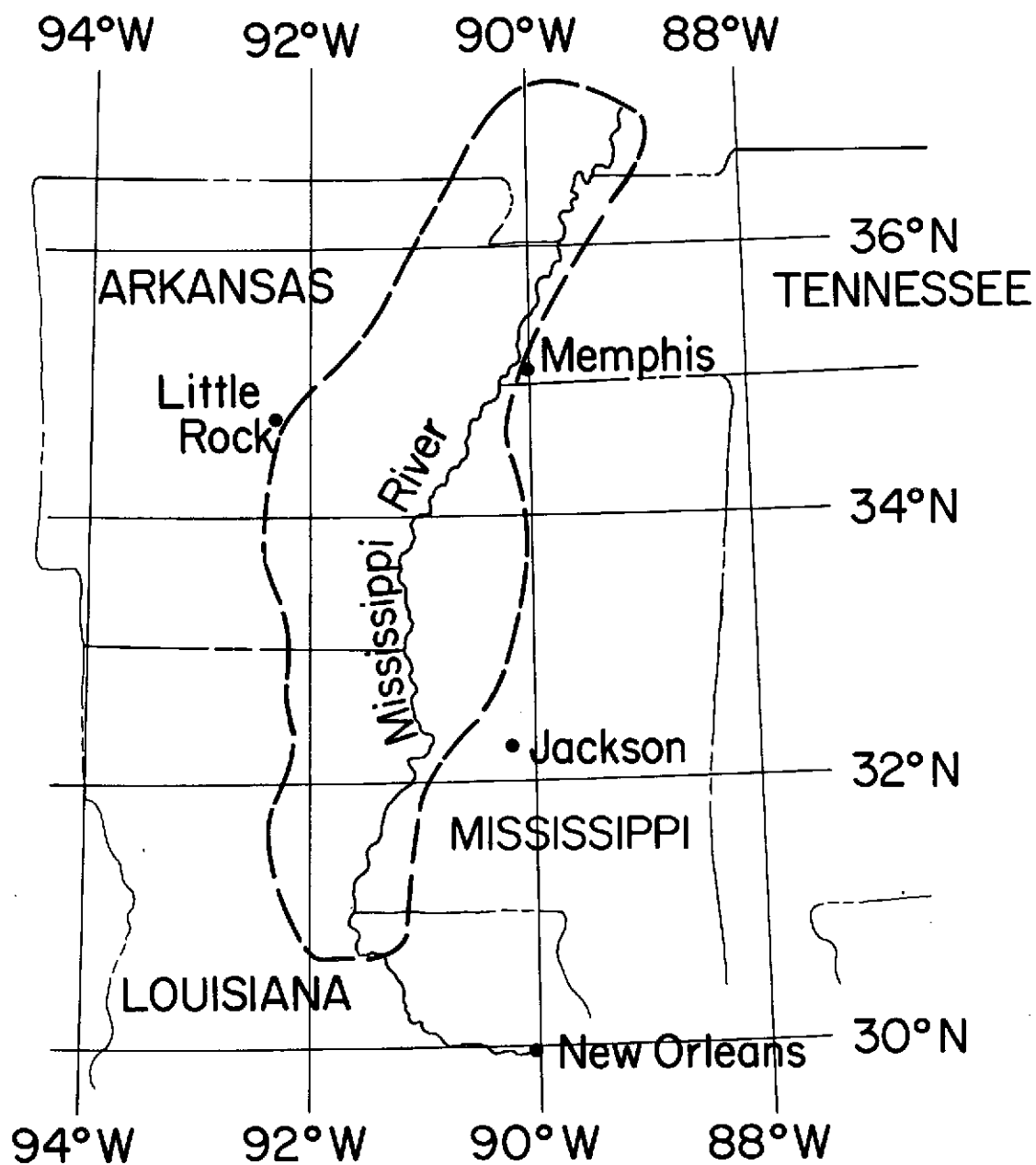


Figure 14. Nimbus 5 ESMR grid print map analysis,
 T_B in $^{\circ}\text{K}$, 1:2.5 Million, Mercator, 1639 to 1643 GMT,
 orbit 569 (day), January 22, 1973, 19.35 GHz.
 (Dotted area: $T_B < 240^{\circ}\text{K}$.)



SOIL MOISTURE PATTERN DETECTED BY NIMBUS 5 ESMR

Figure 15. Map indicating region of outwash aquifers in the Mississippi Valley and approximate area of $T_B < 250^\circ\text{K}$ in the Nimbus ESMR data (Figure 14).

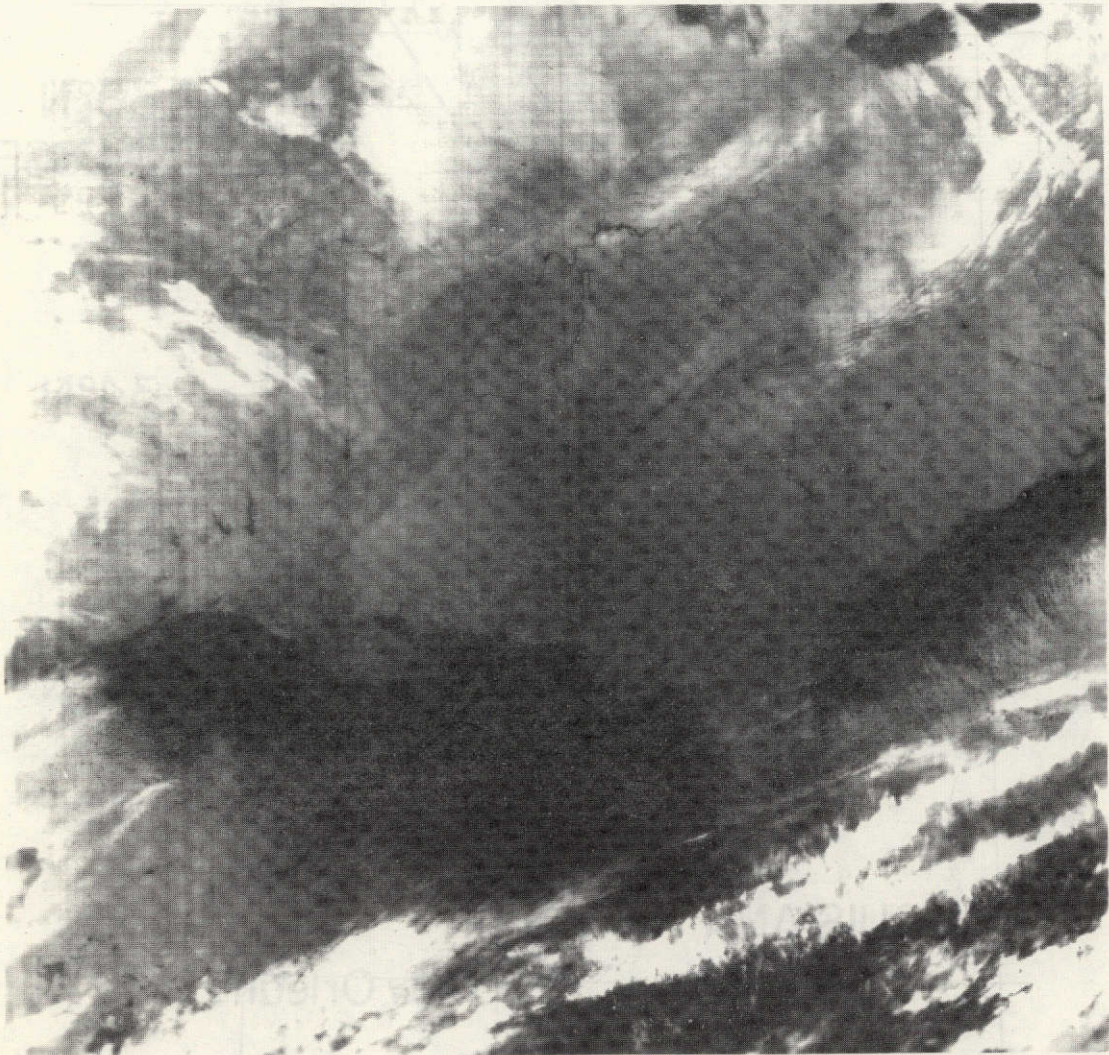


Figure 16. U.S. Air Force Data Acquisition and Processing Program (DAPP) image of IR data (8 to 13 μm), 1205 GMT, December 17, 1972 (1/3 n. mile resolution).

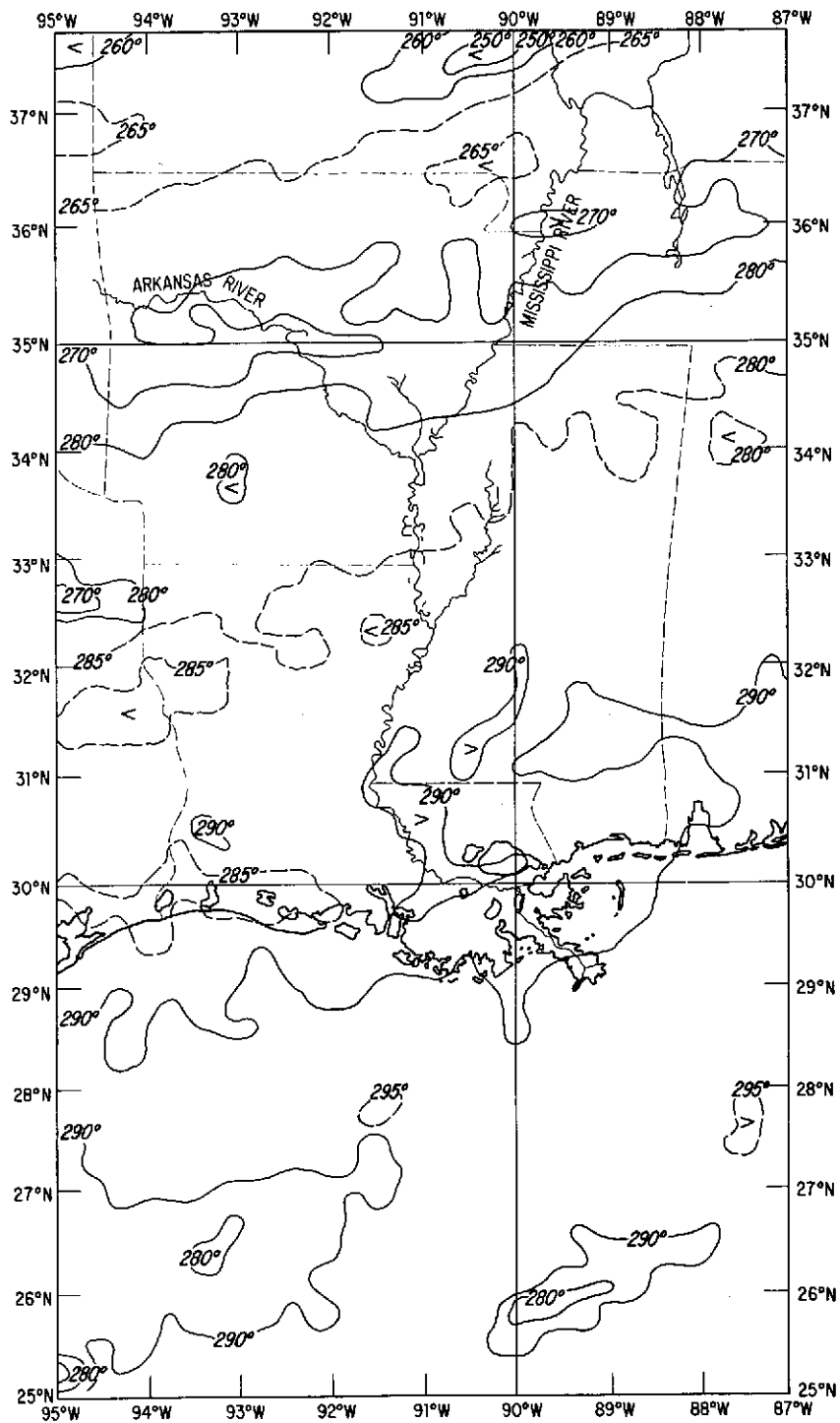


Figure 17. Nimbus 5 THIR grid print map analysis,
 T_B in °K, 1:2.5 Million, Mercator 1639 to 1643 GMT,
 orbit 569 (day) January 22, 1973, $11\mu m$.

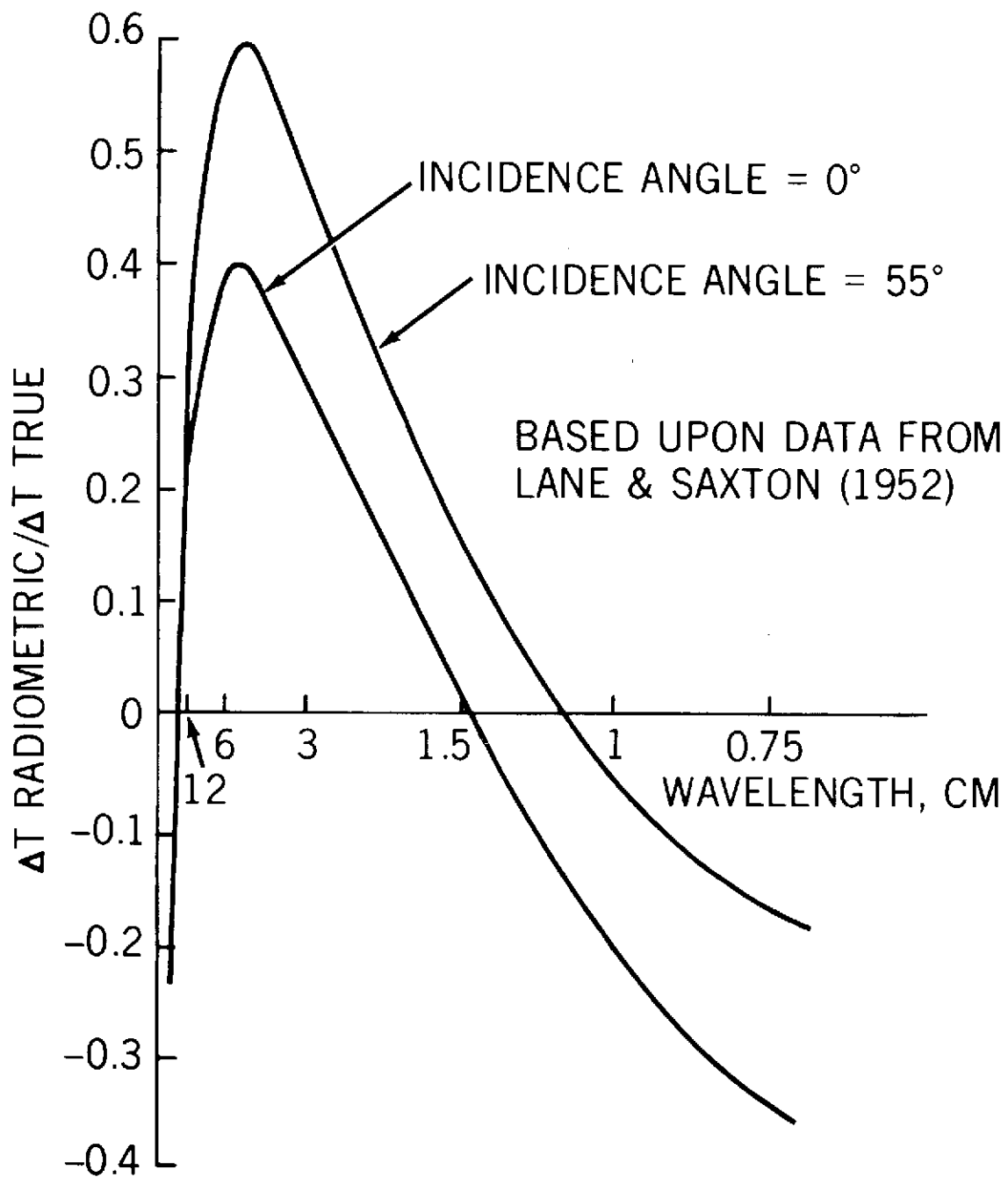


Figure 18. Radiometric Temperature Sensitivity for Calm Seawater, vertically polarized component (average sensitivity in the true range of 273° to 303°K (after Lane and Saxton, 1952).

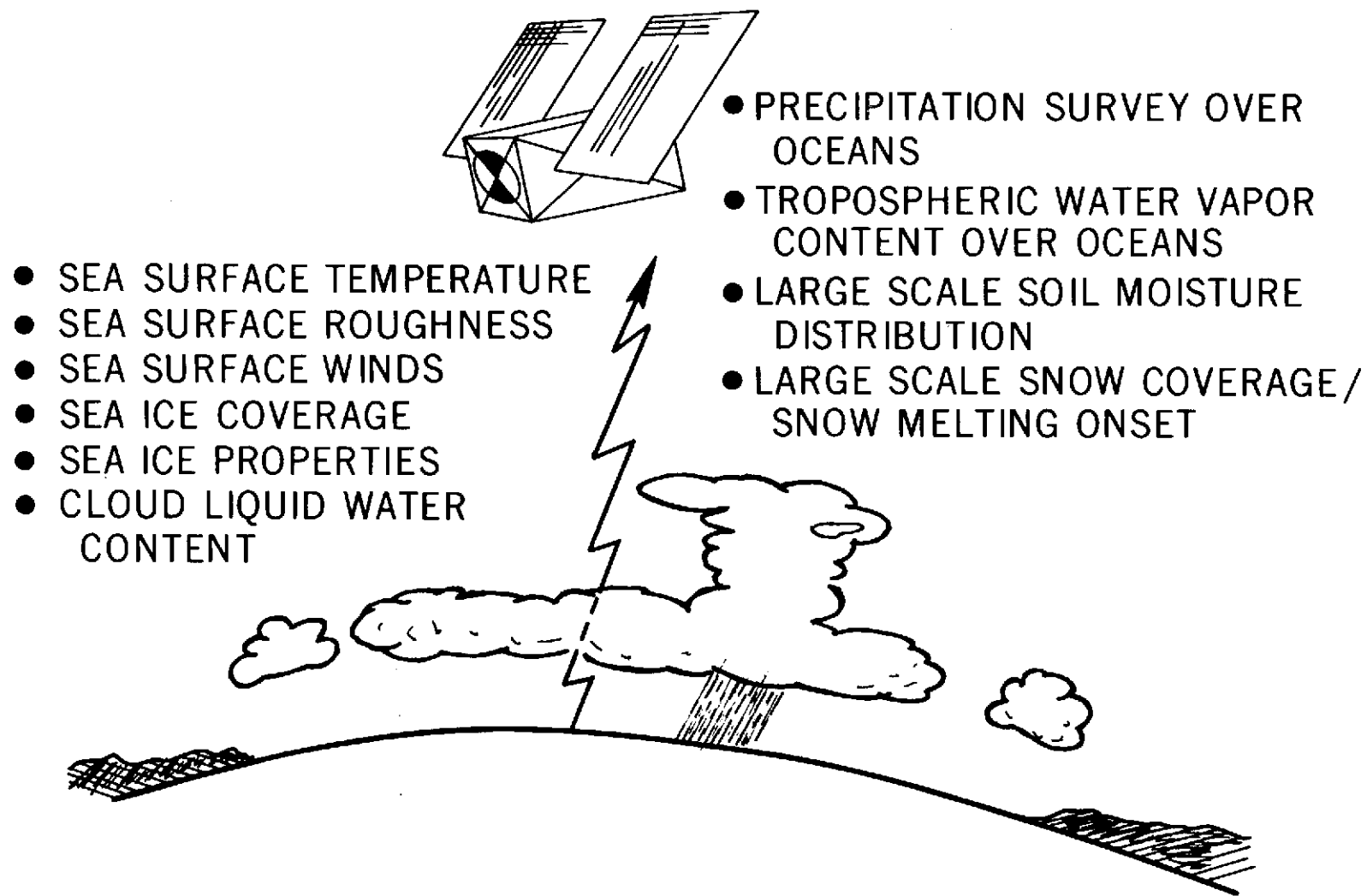


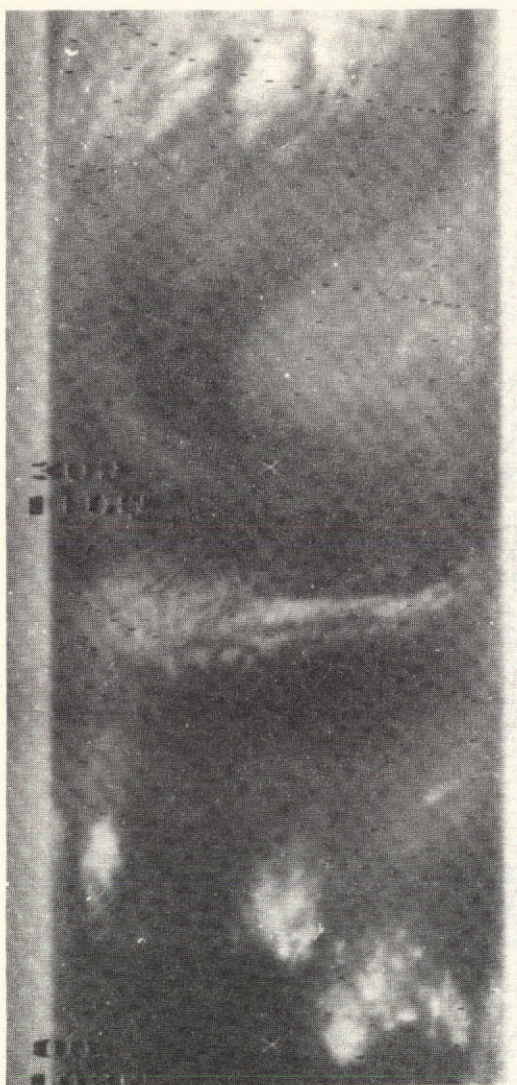
Figure 19. Future meteorological sensing objectives for multi-frequency passive microwave radiometer system.



THIR (6.7μ)
 [200°K TO 270°K]
 [WHITE TO BLACK]

ESMR (19.35 GHz)
 [190°K TO 260°K]
 [WHITE TO BLACK]

Figure 20. Nimbus 5 THIR 6.7μ and ESMR (19.35 GHz) photofacsimile images for 1633 to 1641 GMT, orbit 569 (day), January 22, 1973.



6.7 μ m



11 μ m

Figure 21. Nimbus 5 THIR (6.7 μ m and 11 μ m) photofacsimile images for orbit 570 (day), January 22, 1973.

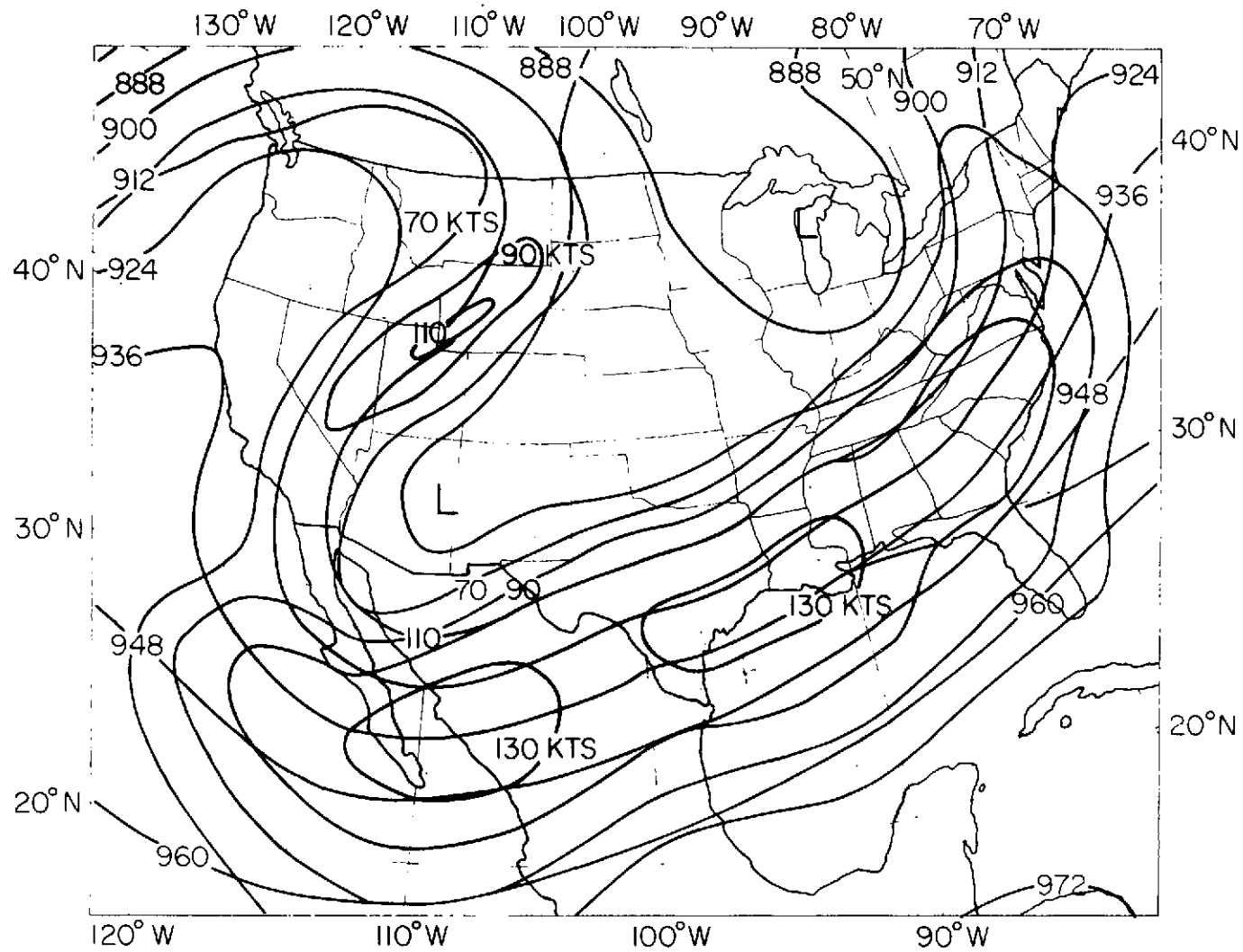


Figure 22. National Meteorological Center, National Weather Service 300 mb chart, for 000 GMT, January 23, 1973. (Light gray tone: 70 to 90 kt isotach, darker gray tone: 90 to >130 kt isotach.)

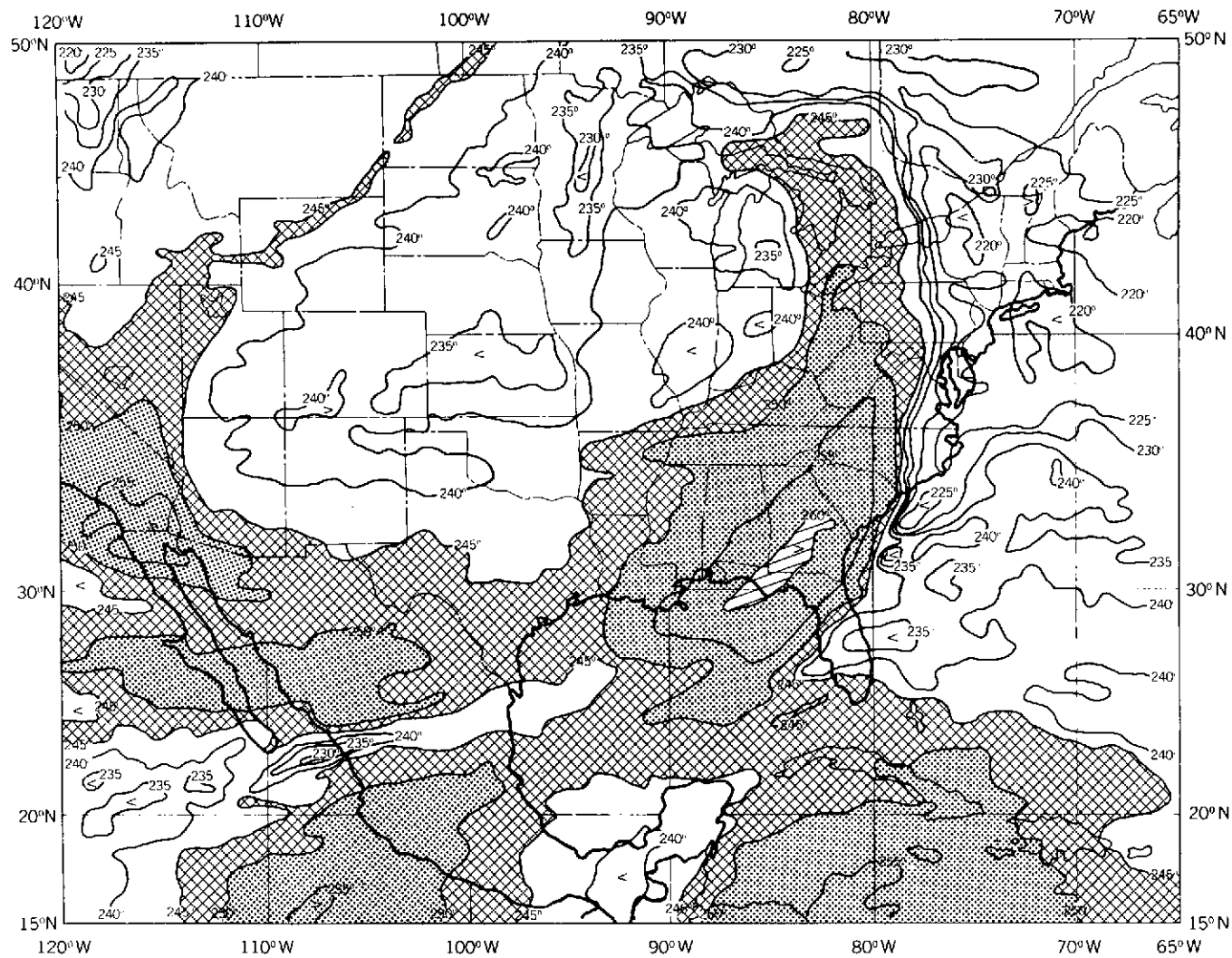


Figure 23. Nimbus 5 THIR ($6.7 \mu\text{m}$) grid print map analysis, T_B in K, 1:2.5 Million, Mercator, 1637 to 1648 GMT, orbit 569 (day), January 22, 1973.

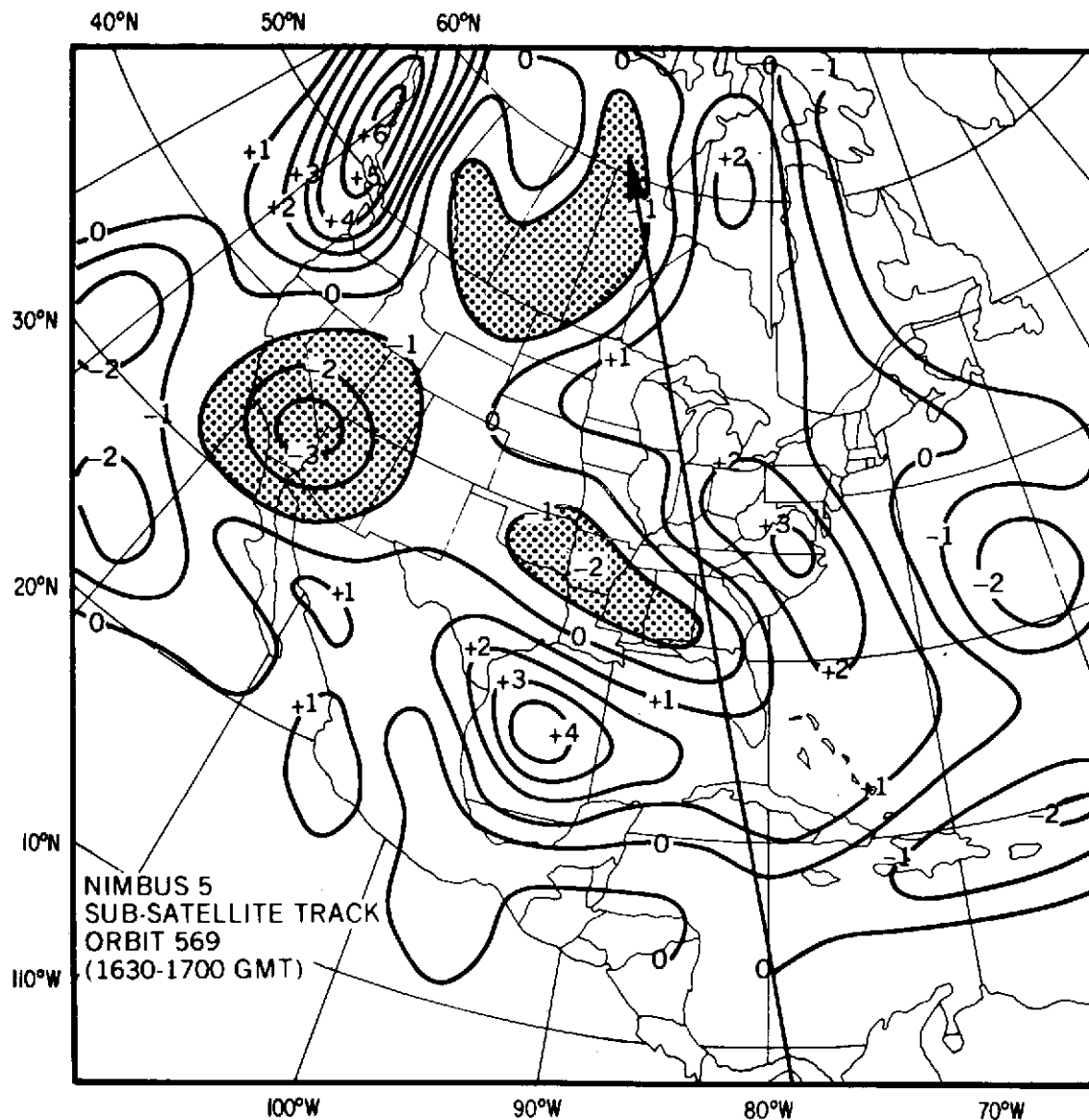


Figure 24. National Meteorological Center, National Weather Service, 650 mb level vertical velocity chart ($\text{microbars sec}^{-1}$), 1200 GMT, January 22, 1973. (Dotted area: $<1 \text{ microbar sec}^{-1}$.)

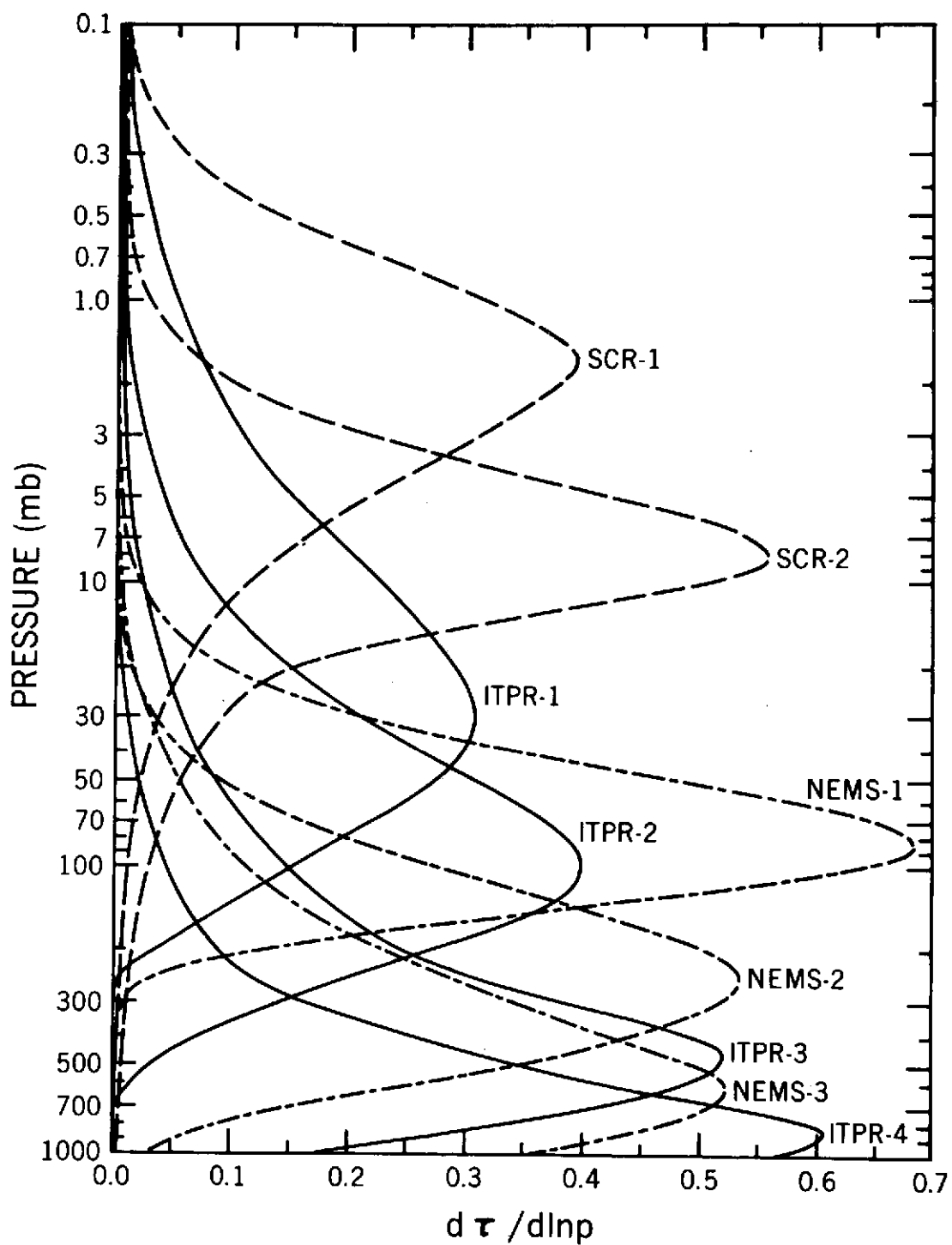


Figure 25. Atmospheric Weighting Function Curves for Nimbus 5 ITPR, NEMS and SCR spectral channels. Derivative of transmittance with respect to the logarithm of pressure (after Smith et al., 1973).

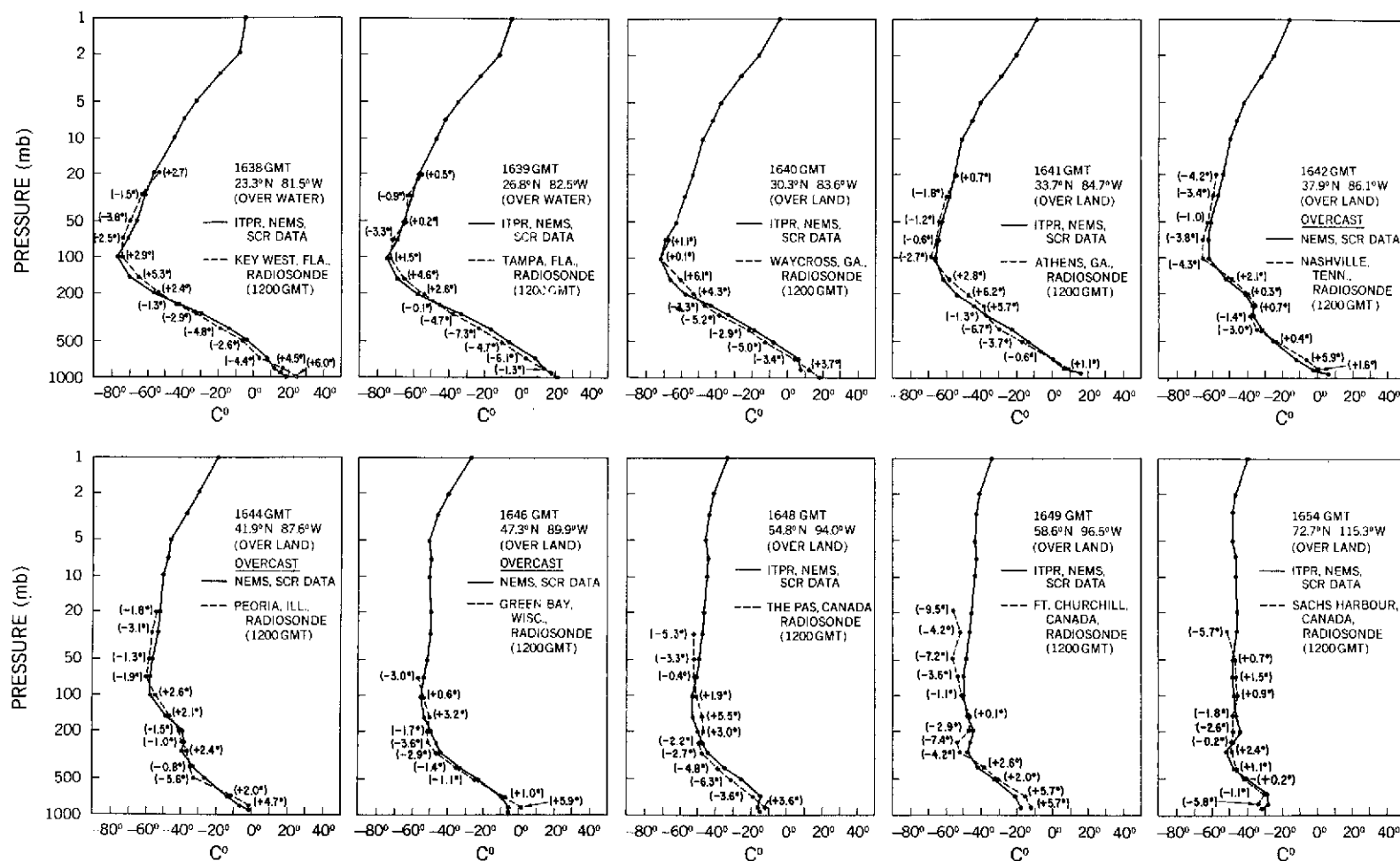


Figure 26. Nimbus 5 Vertical Temperature Soundings derived from ITPR, NEMS and SCR radiances, 1638 GMT to 1654 GMT, orbit 569, January 22, 1973 and related 1200 GMT radiosonde data. (A positive value indicates that the radiosonde air temperature is warmer than the satellite-derived air temperature.)

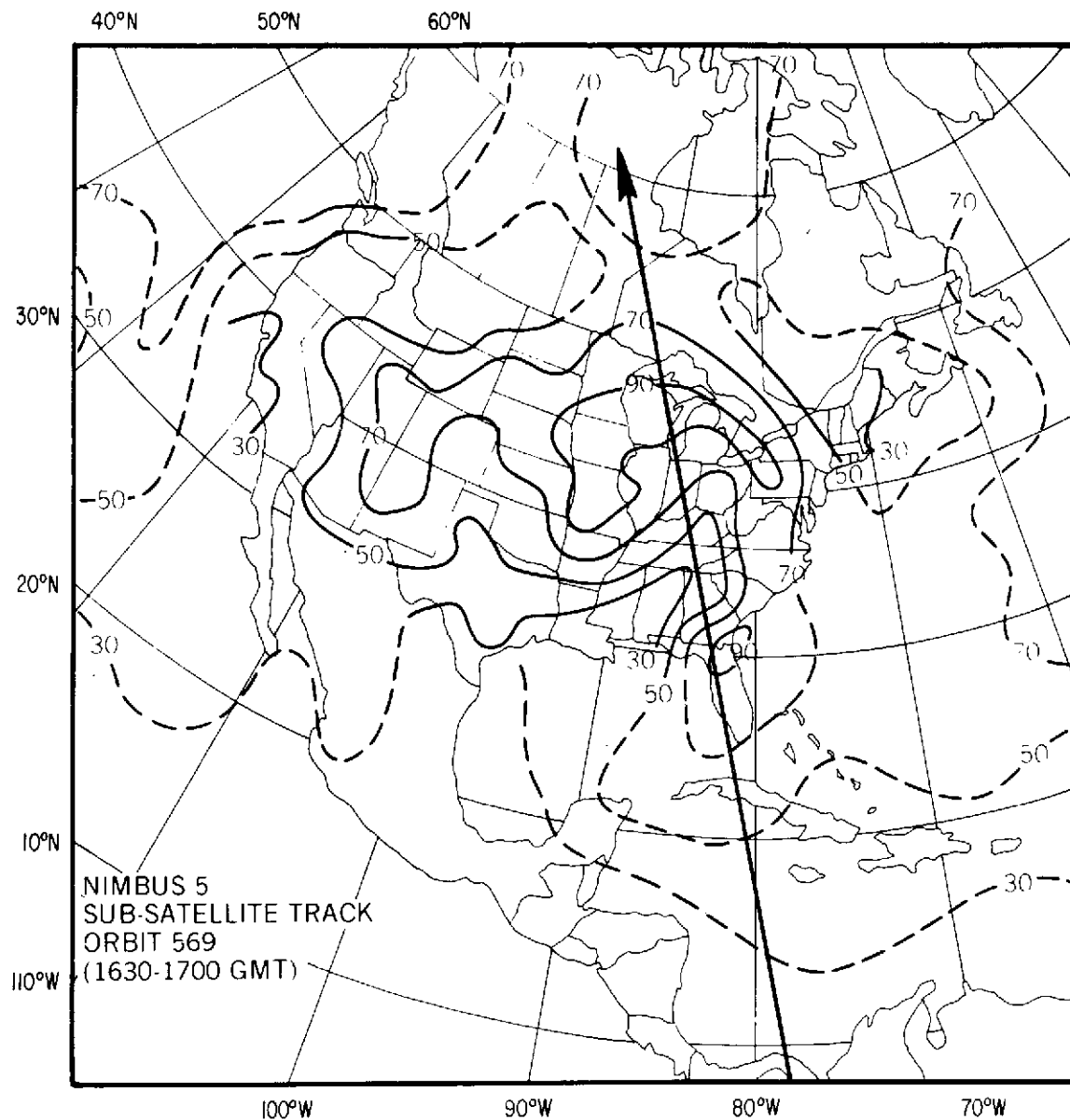


Figure 27. National Meteorological Center, National Weather Service, Average Relative Humidity Chart (%), Surface to 500 mb, 1200 GMT, January 22, 1973.

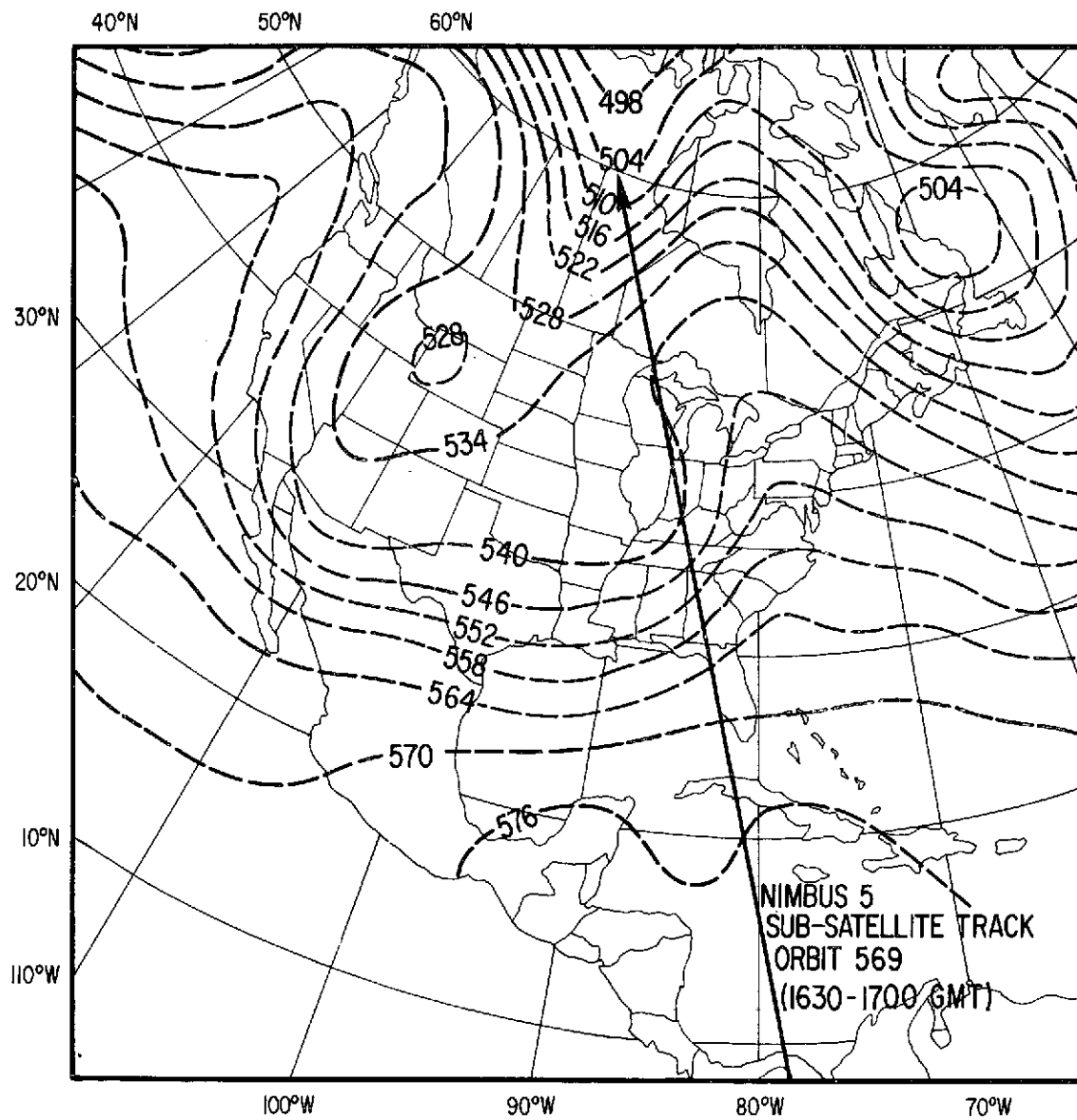


Figure 28. National Meteorological Center, National Weather Service 1000 to 500 mb thickness chart (meters), 1200 GMT, January 22, 1973.